

Wilkinson Microwave Anisotropy Probe (*WMAP*):
Explanatory Supplement¹

The *WMAP* Science Working Group

February 11, 2003

¹Version 1.0

Preface

This document is a concise description of the delivered data sets for the first 12 months of operation of the Wilkinson Microwave Anisotropy Probe (*WMAP*). It is intended as an overview of the delivered sky temperature maps and other data sets and as a description of the specific quantities contained in the *WMAP* time-ordered data. This document also describes the basic architecture and *modus operandi* of the instrument and spacecraft. Detailed descriptions of the spacecraft, instrument and data reduction methods have been described in publications that are referenced throughout this document and in particular at the beginning of Chapter 1.

This document is the cumulative effort of the following people: C. Barnes, C. L. Bennett, M. Greason, M. Halpern, R. S. Hill, G. Hinshaw, N. Jarosik, A. Kogut, E. Komatsu, W. Landsman, M. Limon, S. S. Meyer, M. R. Nolte, N. Odegard, L. Page, H. V. Peiris, D. N. Spergel, G. S. Tucker, L. Verde, J. L. Weiland, E. Wollack, E. L. Wright.

The high quality graphics in this document were created by: B. Griswold and S. J. Bensusen.

Last revised: February 11, 2003

This document is to be referenced as:

Wilkinson Microwave Anisotropy Probe (WMAP): Explanatory Supplement, editor M. Limon, et al (Greenbelt, MD: NASA/GSFC)

Available in electronic form at <http://lambda.gsfc.nasa.gov>

Contents

1	Mission Explanatory Supplement	1
1.1	The Observatory	3
1.2	The Instrument	3
1.2.1	The Optics	3
1.2.2	The Radiometers	4
1.3	The Journey	4
1.3.1	Time Line	6
1.3.2	Launch	6
1.3.3	Deployment and Instrument Power On	7
1.3.4	Observatory Checkout	9
1.3.5	Phasing Loops	9
1.3.6	Earth IR and Outgassing	10
1.3.7	Lunar Fly-by	12
1.3.8	Mid-course Correction	12
1.3.9	Observing Mode	12
1.3.10	Station Keeping	12
1.3.11	Pointing	12
1.4	The Thermal Environment	14
1.4.1	Temperature Monitor Architecture	14
1.4.2	Temperature Monitor Performances	18
1.4.3	Sun Driven Yearly Temperature Changes	20
1.4.4	Aging of Thermal Control Surfaces	22
1.4.5	Operationally Induced Disturbances	23
1.4.6	Radiometric Baselines Discontinuities	24
1.5	The Radiation Environment	26
1.5.1	Plasma Environment	26
1.5.2	Spacecraft Charge Control	26
1.5.3	Solar Flares: Charged Particle Heating	27

2	Data Pipeline	31
2.1	Pre-Processing	31
2.2	Initial Calibration and Map Making	33
2.3	Final Sky Map Processing	34
3	Data Products	36
3.1	Calibrated Sky Maps	37
3.1.1	I Maps (Individual Differencing Assemblies)	37
3.1.2	I Maps (Per Frequency)	38
3.1.3	Smoothed I Maps (Per Frequency)	39
3.2	Derived CMB Products	40
3.2.1	TT Cross-Power Spectra	40
3.2.2	Combined TT Power Spectrum	41
3.2.3	TE Power Spectrum	42
3.2.4	Likelihood Code	43
3.3	Derived Foreground Products	44
3.3.1	Internal Linear Combination Map	44
3.3.2	Foregrounds Derived from Maximum Entropy Method	45
3.3.3	Point Source Catalog	46
3.4	Ancillary Data	47
3.4.1	Intensity Mask	47
3.4.2	Far-Sidelobe Maps	48
3.4.3	Beam Maps	49
3.4.4	Beam Transfer Functions	50
4	Time Ordered Data (TOD)	51
4.1	The Meta Data Table	52
4.2	The Science Data Table	53
4.3	The Analog Instrument Housekeeping (AIHK) Data Table	57
4.4	The Digital Instrument Housekeeping (DIHK) Data Table	58
4.5	The Line-Of-Sight (LOS) Table	59
4.6	Headers	59
5	Software	60
5.1	FITS Readers	60
5.1.1	FITS_READ_MAP	60
5.1.2	FITS_READ_TOD	61
5.2	Pckt2Mnemonic()	61
5.3	Mapping Procedures	63
5.3.1	REPROJ_HEALPIX	63

5.3.2	HEALINFO	64
5.3.3	HEALPIX_Nested_Vectors	64
5.3.4	GRID_OVERLAY	65
5.3.5	CIRCOLOT	66
5.3.6	PLANET_OVERLAY	68
5.4	Transformations	69
5.4.1	TIMETRANSFORM	69
5.4.2	COORTRANS	71
5.5	Widgets	72
5.5.1	MAP_DATE	72
5.5.2	MAPVIEW	72
5.6	WMAP IDL Procedures	73
A	Selected WMAP Log Entries	82
B	Mnemonics Lists	89
B.1	Science Mnemonics	90
B.2	Instrument Housekeeping Mnemonics	91
B.2.1	Amplifier Drain Currents	91
B.2.2	Radiometer RF Bias (Total Power)	92
B.2.3	TRS Temperatures	93
B.2.4	FPA Temperatures	93
B.2.5	RXB Temperatures	94
B.2.6	AEU Temperatures	94
B.2.7	PDU Temperatures	94
B.2.8	AEU Voltages and Reference Roads	95
B.2.9	PDU Voltages	95
C	Acronym List	96

List of Figures

1.1	Spacecraft Overview	2
1.2	Radiometer Schematic	6
1.3	Cool-down Thermal Profile	8
1.4	First Year Thermal Profile	15
1.5	Instrument Temperature Rate Histograms	16
1.6	PRT Noise Power Spectrum	17
1.7	FPA and RXB Temperature Power Spectra	19
1.8	Solar Array Temperature Profile	21
1.9	Solar Flare Effects on the Observatory	29
2.1	Pipeline Overview	32

List of Tables

1.1	<i>WMAP</i> Optical System Parameters	4
1.2	<i>WMAP</i> Feed Specifications	5
1.3	<i>WMAP</i> Radiometer and HEMT Specifications	5
1.4	<i>WMAP</i> Maneuver Summary	10
1.5	Observing Mode Performance	13
1.6	Data Cut Summary	25
1.7	Solar Storms	28

Chapter 1

Mission Explanatory Supplement

The *WMAP* (Wilkinson Microwave Anisotropy Probe) mission is designed to determine the geometry, content, and evolution of the universe via a 13 arcminute FWHM resolution full sky map of the temperature anisotropy of the cosmic microwave background radiation. The choice of orbit, sky-scanning strategy and instrument/spacecraft design were driven by the goals of uncorrelated pixel noise, minimal systematic errors, multifrequency observations, and accurate calibration. The skymap data products derived from the *WMAP* observations have 45 times the sensitivity and 33 times the angular resolution of the COBE DMR mission.

An overall description of the *WMAP* mission can be found in Bennett et al. (2003a). Details of the instrument design are described in Jarosik et al. (2003a), Page et al. (2003c), and Barnes et al. (2002). The basic results from the first year of *WMAP* observations are described in Bennett et al. (2003b).

Jarosik et al. (2003b) describes the in flight performance of the *WMAP* radiometers. Characteristics of the telescope beam profiles and limits on systematic effects are provided in Page et al. (2003a) and Barnes et al. (2003). A summary of non-cosmological signals observed is presented in Bennett et al. (2003c). Hinshaw et al. (2003a) provides details on the data analysis pipeline and uses the results of the previous four papers.

The methods for obtaining cosmological parameters are described in Verde et al. (2003). Limits on non-Gaussian fluctuations are provided in Komatsu et al. (2003). The angular power spectrum and basic cosmological parameters resulting from *WMAP* are presented in Hinshaw et al. (2003b)

and Spergel et al. (2003). The observed TE polarization signal is described in Kogut et al. (2003). The implications of the above results for inflation is described in Peiris et al. (2003). Finally a guide to understanding how cosmological parameters affect the the observed power spectra is provided in Page et al. (2003b).

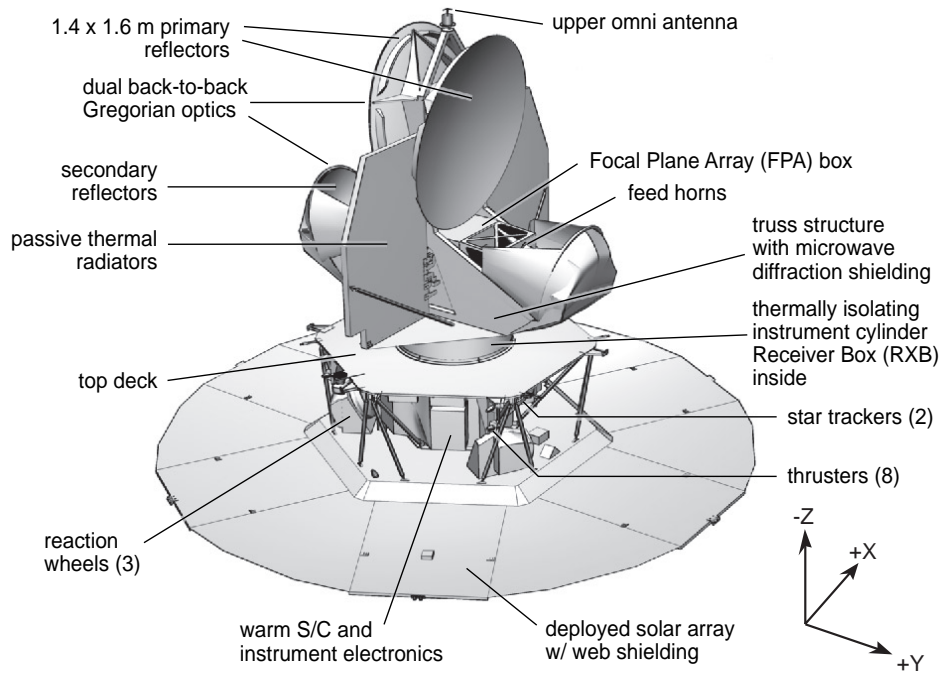


Figure 1.1: Spacecraft Overview. View of the spacecraft in the deployed configuration with major components labeled. The primary and secondary reflectors as well as the two thermal radiators are clearly visible in the upper portion of the image. The cold and warm section of the radiometers are housed in the FPA and RXB respectively and are located in the core of the spacecraft under the primary reflectors. All the support electronics (AEU, DEU, PDU, MAC, LMAC), gyros, star-trackers, and reaction wheels are mounted on the hexagonal hub at the base of the spacecraft. While at L2, the optics, instrument and support electronics are constantly in the shade of the solar array and never exposed to solar radiation.

1.1 The Observatory

The design of the *WMAP* observatory¹, the choice of its orbit and its operational mode has been driven by the mission's science requirements of producing full sky maps of the cosmic microwave background radiation of unprecedented accuracy. Therefore the overall mission's design philosophy has been to minimize and control systematic errors even at the expense of sensitivity, simplicity and cost. This choice has a profound effect not only in the design of the instrument but on the spacecraft as well. In particular, to minimize temperature variations in the optics and the radiometers that could lead to systematic effects in the measured signals the thermal control is entirely passive. The heat generated by the instrument is radiatively dissipated by two large radiators mounted in the upper part of the spacecraft (see Figure 1.1) while all the support systems (battery, analog and digital electronics, etc.) are mounted around an open hexagonal hub in the lower part of the spacecraft and dissipate their excess heat through individual radiating surfaces which are part of their enclosures.

1.2 The Instrument

The *WMAP* instrument is basically made by two separate but highly interdependent components:

- **The Optics** focus the incoming radiation in the focal plane.
- **The Radiometers** amplify and convert the microwave signal into a measurable voltage.

In the following section we briefly describe the basic details of each of this components, we will also briefly describe the spacecraft's thermal design.

1.2.1 The Optics

The *WMAP* optical system consists of two back-to-back shaped offset Gregorian telescopes (see Figure 1.1). This is a highly symmetrical and compact optical design allows efficient placement of the feeds and radiometers while at the same time meeting all the science requirements. A summary of the optical system basic parameters is given in Table 1.1. The *WMAP*'s optical system design and characterization is described in detail in Page et al. (2003c)

¹The combination of the spacecraft and the instrument are referred to as the observatory throughout this document.

Two mirror-symmetric arrays of corrugated feeds couple the radiation from *WMAP*'s two telescopes to the inputs of the differential receivers. Corrugated feeds were chosen because of their low emissivity, symmetric beam pattern, and low sidelobes. A summary of the feed basic parameters is given in Table 1.2. The *WMAP*'s feeds design, manufacturing methods, and characterizations are described in details in Barnes et al. (2003)

1.2.2 The Radiometers

The 20 differential radiometers that make up the *WMAP* instrument cover 5 frequency bands and share the same design: they are pseudo-correlation differential radiometers with High Electron Mobility Transistor (HEMT) amplifiers passively cooled to ~ 90 K. A summary of the *WMAP* radiometers design parameters and a schematic of an individual radiometer are given in Table 1.3 and Figure 1.2 respectively. The *WMAP* radiometers are described in detail in Jarosik et al. (2003a)

1.3 The Journey

This section summarizes the events and the environment encountered by the observatory from days immediately preceding launch to the moment of the lunar swing-by that provides the gravity assist to reach its final orbital

Band	K	Ka	Q	V	W	
Optical System			Gregorian			[-]
Primary Dimensions			1.4 \times 1.6			[m]
Secondary Dimensions			0.8 \times 0.8			[m]
Focal length			90			[cm]
Beam Size	0.88	0.66	0.51	0.35	0.22	deg
Max Edge Taper	-13	-20	-21	-21	-16/-20	[dB]
Forward Beam Efficiency	0.960	0.986	0.986	0.996	0.996/0.999	[-]

Table 1.1: *WMAP* Optical System Parameters. The beam patterns are not Gaussian, and thus are not simply specified. The size given here is the square-root of the beam solid angle. The value reported for the edge taper is the maximum for the center of the band. As the feeds are not illuminating the reflectors symmetrically, most of the edge has a substantially smaller taper. The beam efficiency is the integral of the beam in the area around 2° from the minimum divided by 4π ; a value of 0.960 means that 4% of solid angle is scattered into the sidelobes.

Band	K	Ka	Q	V	W
Waveguide (WR)	42	28	22	15	10
ν (GHz)	19.5–25	28–37	35–46	53–69	82–106
ν_{gv} (GHz)	22	25.9	32.5	49.1	90.1
Length (mm)	536.4	542.1	567.6	569.6	603.3
Throat \varnothing (mm)	12.50	8.34	6.68	4.41	2.97
Aperture \varnothing (mm)	109.37	89.92	89.88	59.89	39.92
Mass (g)	1010	650	615	325	214
N_{gv}	116	169	217	329	533
N_s	1	1	3	4	5
θ_{fwhm} (deg)	10.1–7.7	8.9–6.7	7.8–6.0	8.8–7.4	9.7–8.3
Gain (dBi)	24.9–28.1	26.1–29.1	27.3–30.8	26.0–28.8	25.0–27.2

Table 1.2: *WMAP* Feed Specifications. The waveguide bands listed are for the rectangular commercial standard designations used in the radiometer, ν_{gv} is the hybrid frequency, N_{gv} is the total number of corrugations, and N_s is the number of sections (1 meaning made in one piece). The antenna beam width and the gain values range from the lower to the higher ends of the band.

<i>WMAP</i> Band Designation	K	Ka	Q	V	W
Radiometers Specifications					
Frequency Range (GHz)	20 – 25	28 – 36	35 – 46	53 – 69	82 – 106
$\Delta\nu_{eff}$ (GHz)	4	5	8	13	19
Number of Radiometers	2	2	4	4	8
Sensitivity (mK sec ^{1/2})	0.65	0.78	0.92	1.13	1.48
T_{sys} (K)	29	39	59	92	145
HEMTs Specifications					
Noise temperature @300K (K)	~100	~115	~150	~260	~370
Noise temperature @85K (K)	30±2	33±3	48±5	64±7	96±7
Gain @300K (dB)	33	32	31	31	32
Gain @85K (dB)	34	34	34	35	35
Gain flatness (dB)	±1.5	±1.0	±1.5	±2.5	±3.0

Table 1.3: *WMAP* Radiometer and HEMT Amplifiers Specifications. The sensitivity is per radiometer. Sensitivity and T_{sys} values are given in Rayleigh-Jeans temperature.

position around L2.

1.3.1 Time Line

The *WMAP* observatory was powered on and tested for the last time at GSFC on April 6, 2001 before being shipped to Kennedy Space Center (KSC) on April 18 where it arrived two days later. In the approximately two months following its arrival at KSC, the observatory underwent further testing, integration with the launch vehicle 3rd stage and finally integration with the rest of the launch vehicle. The launch vehicle was a Boeing Delta II 7425. This was the 286th Delta launch. A summary of these events are included in the log in Appendix A which also covers the rest of the mission to the end of the first year of science observations.

1.3.2 Launch

On June 30, 2001 at 19:29 GMT the GSFC control team gave its approval to proceed with the terminal count-down. Approximately 10 minutes later the observatory was switched to internal power and at 19:46:46 GMT it lifted off from launch pad 17B at the Eastern Range Space Launch Complex – the first step in a journey that took it three times around the Earth (phasing loops)

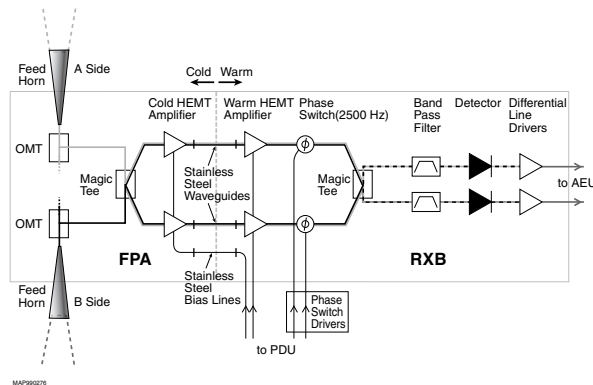


Figure 1.2: Layout of an Individual *WMAP* Radiometer. Components on the cold (left) side of the stainless steel waveguides are housed in the FPA where they passively cooled to ~ 90 K through thermal links to the radiator panels. The components in the RXB achieve a balance temperature of ~ 290 K.

and close to the Moon (fly-by) before it reached its intended observational position around L2.

Five minutes after launch, the Delta II first-stage engine cut off and the fairing jettisoned, exposing the observatory for the first time to the full space environment. Although the launch vehicle was tracked by radar station and its telemetry was received by the Boeing launch team, there was no contact with the observatory itself during launch and ascent. At approximately 21:00 GMT the signal from of *WMAP*'s omni-directional was picked up by NASA's TDRS-W satellite and relayed to the ground, confirming that the payload was in good health and that all parameters were nominal. The *WMAP* payload was successfully inserted in a ~ 185 km elliptical parking orbit with a $\sim 28.7^\circ$ inclination.

1.3.3 Deployment and Instrument Power On

From the moment the observatory was switched to internal power, 5 minutes before launch, until deployment of the solar array panels, the observatory relies on power provided by the battery. At 21:03 GMT an on-board procedure triggered the deployment of the solar array. Immediately after this event the spacecraft oriented itself along the Sun-line maximizing the electrical power being generated by the array and, at the same time, protecting the instrument from the solar radiation.

At 21:43 GMT the *WMAP* instrument was powered in flight for the first time: housekeeping data was monitored as the instrument cooled and the flight burn-in phase was completed as scheduled. All science signals were within nominal limits during the cool down period. HEMT drain currents and RF radiometer total power were similar to the modeled response based upon the thermal environment and the radiometric flux presented to the instrument. The RXB temperature peaked at ~ 293 K before cooling as anticipated due to the instrument power on time, thermal loads, and cooling profile. No anomalies were noted in the instrument electronics system (AEU/DEU and PDU) performance.

A platinum resistance thermometer (PRT) on top of the thermal reflector system radiator (DTAMXTOPRADT) failed on 2001:185:1100 GMT. From the flight telemetry we conclude that the sensor failed open and remains in this state. This failure was not completely unexpected, a similar sensor at the same location had failed during ground testing. Two days after deployment on July 2, 2001 at 19:18 GMT the spacecraft entered observing mode for the first time.

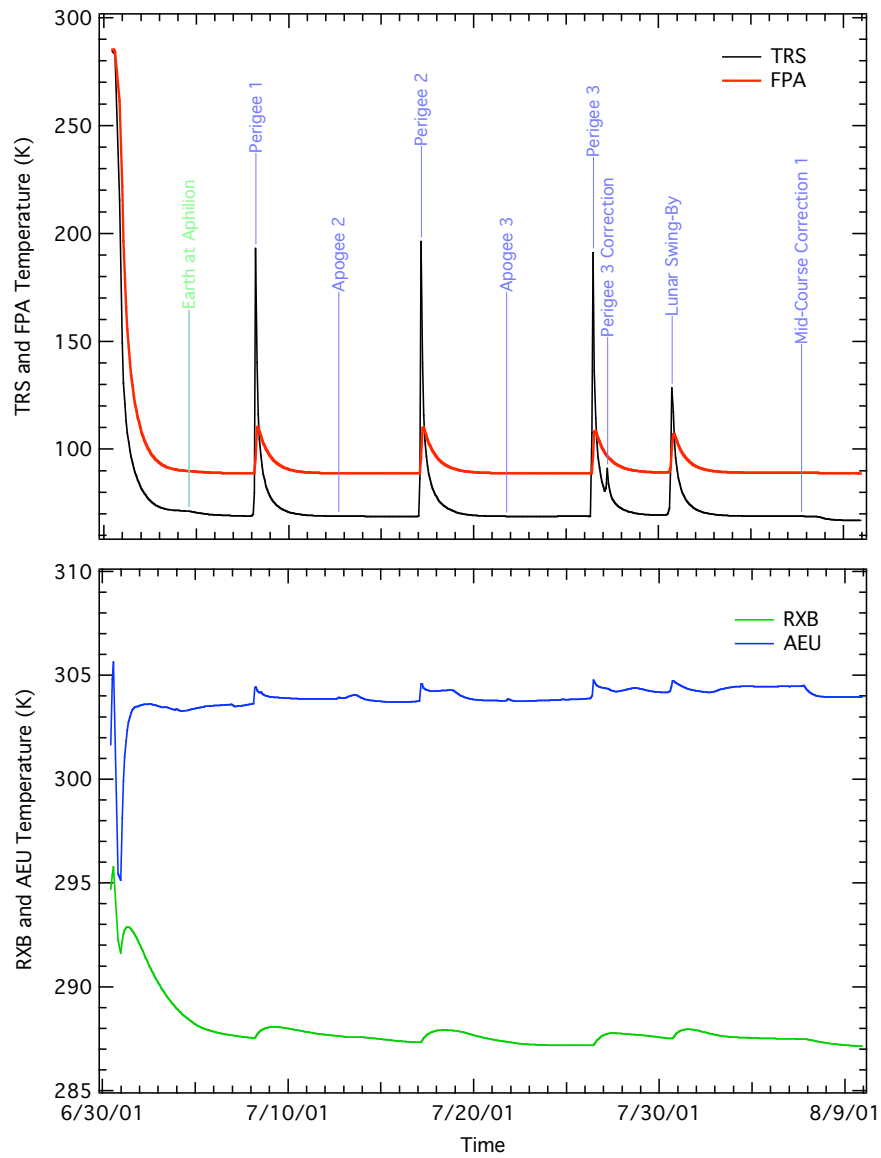


Figure 1.3: Cool-down Thermal Profile. Thermal profile of major instrument subsystems (TRS, FPA, RXB and AEU) from the launch to the beginning of the observations used for the first year maps.

1.3.4 Observatory Checkout

From June 30, 2001, when *WMAP* was launched, to August 17, 2001 the *WMAP* spacecraft and instrument underwent a period of formal checkout. During this period the spacecraft was contacted through the DSN multiple times each day and all subsystems were tested thoroughly. The end of the in-flight checkout marked the beginning of normal mission operations; during this time the spacecraft is constantly in observing mode with one DSN contact per day. The spacecraft exits observing mode only for the planned station keeping maneuvers (see section 1.3.10) or if an unexpected event (see Table 1.7) puts it in “Safehold”. Details of the spacecraft in-flight checkout are presented in Jackson (2002).

1.3.5 Phasing Loops

Three orbital phasing loops and a lunar gravity assist were employed to perform the transfer to the mission’s operational orbit – a Lissajous orbit about the Sun-Earth L2 Lagrange point, ~ 1.5 million km from Earth in the anti-Sun direction. To fine tune the spacecraft trajectory in preparation for the Lunar Fly-by, 7 burns were performed while at Earth’s perigee (4) and apogee (3).

Thruster calibration maneuvers were performed at apogees. This allowed calibration of the propulsion system using the thruster configurations for the phasing loop and station keeping burns.

A summary of the phasing loops maneuvers as well as all the other maneuvers performed during the first year of the *WMAP* observatory’s operations are given in Table 1.4. The first perigee burn (P1) was the first of a series of incremental adjustments of the satellite’s orbital energy and phasing for the final lunar assist. The second perigee burn (P2) provided a slight correction in preparations for the critical final perigee burns. The velocity boost provided by the final perigee (P3) and final correction (P3c) burns tuned the orbit for a lunar encounter at the desired time and location to achieve the desired eclipse free trajectory (i.e. an orbit that does not cross Earth-shadow’s cone). The temperatures of the primary reflectors exhibited significant transients during the perigee passes (see Figure 1.3) as they were exposed to both Earth IR inputs and edge-on solar inputs to the upper portion of their +X sides. This was an anticipated aspect of the mission design.

The phasing loops were also used to measure the far side-lobe response of the *WMAP* optical system. See Barnes et al. (2003) for details. In particular

during the first orbital phasing loop (July 2-8, 2001), while the Moon was close enough to be a significantly bright thermal source, the spacecraft was operated in a scanning pattern very similar to the flight observing mode with the Moon sweeping through the optical system far side-lobes.

1.3.6 Earth IR and Outgassing

The materials and processes used in the construction of the *WMAP* Observatory result in a small mass loss due to outgassing. Outgassing from and re-deposition of materials on spacecraft surfaces are anticipated in flight due to the loss of volatile materials and the pre-flight exposure to the ambient environment. Outgassing products emitted and re-encountered by spacecraft have a finite capture probability which increases upon cooling. Pre-flight contamination estimates did not indicate a concern for critical passively-cooled elements and optical sensors. In-flight performance of these subsystems are consistent with these estimates. In flight, outgassing by-products resulted in a small but detectable perturbation on the system's total angular momentum during perigee maneuvers (Starin et al., 2002). This observation may be of potential interest to the mission design of spacecraft with large cold surfaces.

Prior to each perigee maneuver, *WMAP* was in its nominal science observing mode. The first command to prepare for a burn maneuver placed

Event	yyyy:ddd:hhmm GMT	ΔV (m/s)	Burn (s)	Altitude (km)
Apogee 1	2001:185:1322	1.921	106	299,478 (E)
Perigee 1	2001:189:0433	20.194	1274	3,098 (E)
Apogee 2 (+Z Cal)	2001:193:1611	0.254	41	347,891 (E)
Perigee 2	2001:198:0336	2.514	177	2,955 (E)
Apogee 3 (-Z Cal)	2001:202:1854	0.296	40	356,012 (E)
Perigee 3	2001:207:1029	7.410	546	4,741 (E)
Perigee 3 Correction	2001:208:0430	0.308	24	158,306 (E)
Lunar Swing-By	2001:211:1637	N/A	N/A	5,279 (M)
Mid-Course Correction 1	2001:218:1637	0.103	18	755,736 (E)
Mid-Course Correction 2	2001:257:1637	0.042	6	1,402,107 (E)
Station Keeping 1	2002:016:1650	0.428	72	(L2)
Station Keeping 2	2002:128:1603	0.348	49	(L2)
Station Keeping 3	2002:211:1638	0.460	66	(L2)

Table 1.4: *WMAP* Maneuver Summary. The altitude in the last column is measured either respect to the surface of the Earth (E) or Moon (M).

the system into Inertial Mode. Once in this configuration for the perigee pass, the spacecraft and its solar array panels were oriented approximately 45-to-50 degrees from the Sun-line and the instrument was directed toward the nadir. This placed the thrusters in the proper orientation for the burn. These conditions also result in an attitude profile which allows the Sun to briefly heat portions of the instrument and the Earth albedo to illuminate the anti-solar side of the array before perigee. At the first perigee, a torque of 0.004 Nm and a peak system momentum of 2 Nms were noted before the ASC returned to nominal state. (Note: The maximum allowed wheel torque and momentum are 0.215 Nm and 10 Nms respectively. If these values are exceeded then the on-board software invokes “Safehold” mode. The wheels can store a total momentum of ± 75 Nms. The event did not pose a performance problem for the ACS at any time.)

To understand this small perturbation on the ACS response, we recall that once the solar arrays are deployed the heavily insulated backside, which forms a solar shield for the instrument, rapidly cools to space. By design, this protects the *WMAP* telescopes from millimeter wave emission from the Sun and reduces the instrument’s thermal load to facilitate passive cooling. The solar shield fills approximately one-third of the spacecraft central truss field-of-view. As a result, these cooled surfaces serve as a collection point for outgassing by-products from the central hub electronics, blanketing, and vent paths from the warm portions of the instrument. Based upon the pre-launch configuration, we estimate a mass of ~ 0.8 kg settles on the back of the solar shield in flight. The dominant outgassing component, water, has sufficient energy to be liberated in high vacuum when warmed above 130 K.

Thermal sensors indicate that the Earth infrared exposure was sufficient to sublimate water on the back of the solar shield during the perigee maneuvers. Due to shadowing of Earth IR by the instrument and central hub, the release of the material on the back of the solar array panel was delayed in time. The resultant imbalance in the sublimation rate across the array is consistent with the observed torque magnitude and profile. This basic hypothesis is supported by telemetry from the coarse sun sensors (CCS) and subsequent analysis of *WMAP*’s trajectory. The mass of the sublimate material for each perigee event and ~ 9 day outgassing time constant derived from the telemetry are compatible with the anticipated range of parameters for the *WMAP* observatory. The time between perigee maneuvers and subsequent heating events enabled $\sim 97\%$ of the outgassing products to be dumped from the solar shield before proceeding to L2.

1.3.7 Lunar Fly-by

Although the propulsion system was passive during the lunar swing-by, the encounter has a large influence on the satellite's final trajectory. On July 30, 2001 at 16:37 the lunar swing-by occurred as planned.

1.3.8 Mid-course Correction

To correct the growth of errors from the nominal trajectory to the L2 Lissajous orbit, two mid-course correction (MCC1 and MCC2) burns were planned and executed prior to the first Jupiter beam calibration season. This approach allowed minimal propellant usage and minimized the potential disruption during main beam mapping using Jupiter. The thermal stability of the observatory was sufficiently stable to begin collection of science data on 2001:222 (08/10/2001).

1.3.9 Observing Mode

The spacecraft has six operational modes (see Bennett et al. (2003a) for details) but it spends more than 99% of the time in observing mode. While in observing mode, the spacecraft spins around its vertical (Z) axis every 129.3 s while the Z axis precess around the around the Sun-line every 1 hour described by cone with an half-angle of 22.5° . This compound motion is achieved varying the speeds of the 3 reaction wheels mounted symmetrically around the spacecraft's lower deck (see Figure 1.1). Excess momentum is unloaded during the station keeping maneuvers.

1.3.10 Station Keeping

Three station keeping (SK1, SK2, and SK3) burns were performed to maintain the desired orbit. During these maneuvers the satellite is de-spun to operate in Delta-V mode. Station keeping maneuvers are designed to minimize thermal disturbance and duration. The science data is suitably flagged in the archive to indicate these activities. A list of the station keeping maneuvers is included in Table 1.4.

1.3.11 Pointing

The *WMAP* observatory orientation is controlled by a redundant attitude control system (ACS) which integrates the signals from multiple sensors through a Kalman filter and acts upon a set of reaction wheels and thrusters

to maintain the desired spacecraft operational mode. The attitude control system sensors component suite includes:

- Course Sun Sensor (CCS)
- Digital Sun Sensor (DSS)
- 2 Two-Axis Rate Assemblies (TARAs) or Gyroscopes
- 2 Autonomous Star Trackers (ASTs)

Three reaction wheels provide attitude control and an eight thruster (2 roll, 2 pitch, 2 yaw, and 2 backups) propulsion system provides the orbit adjustment capabilities needed to achieve and maintain the correct L2 trajectory. The eight thrusters are also used for attitude control during the orbit maneuvers and for unloading any system momentum buildup on the spacecraft.

WMAP's ability to reconstruct a full map of the sky from a series of differential measurements depends greatly upon the observatory capability of maintaining a stable highly, inter-linked observing pattern. The motion of the *WMAP* observatory is specified in terms of 3-1-3 Euler angles and rotations specified in *WMAP*'s rotating sun reference (RSR) frame. Because the Z axis of the RSR frame is defined as the vector from *WMAP* to the Sun, the three Euler angles are defined as follows: ϕ , the precession angle about the Sun-line; θ , the angle between the spacecraft Z axis and the Sun-line; and ψ , the spin angle about the spacecraft Z axis. The performance requirements for observing mode are specified in terms of the ϕ and ψ rates and the θ angle. Table 1.5 shows the observing mode requirements and the in-flight measured performance.

Euler States	Requirements	Pre-Calibration	Post-Calibration
ϕ precession rate (deg/s)	$-0.1 \pm 6.3\%$	$-0.1 \pm 9\%$	$-0.1 \pm 3.6\%$
θ (deg)	22.5 ± 0.25	22.5 ± 0.064	22.5 ± 0.0234
ψ spin rate (deg/s)	$2.784 \pm 5\%$	$2.784 \pm 0.32\%$	$2.784 \pm 0.13\%$

Table 1.5: Observing Mode Performance. The pre-calibration data were measured in flight but using the default calibration coefficients loaded in the ACS before launch. The post-calibration coefficients were uploaded on August 9, 2001, at the end of the in-flight checkout.

1.4 The Thermal Environment

While a platform at L2 is certainly a much better place than Earth orbit for conducting CMB observations, it is still slightly affected by some solar induced disturbances. In this section we describe such disturbances and the effects that they have on the instrument stability.

Thermal data from the *WMAP* observatory not only provides a means of monitoring the health and safety of the various on-board systems, but enables one to search for and understand potential instrumental systematic effects. Detailed knowledge of the thermal performance of the observatory in flight is important in assessing the quality of the end data products.

In practice, *WMAP* maintains thermal equilibrium by balancing the absorbed solar radiation input and on-board electrical power dissipation with passive radiative cooling to space. The temperature of the entire spacecraft is extremely uniform due to the vehicle's orbital geometry, constant spin/precession rates and stable power draw. The dominant mechanism that drives changes in the system's temperature is the variation of spacecraft-to-sun separation as a function of orbital position; however, operationally induced changes in spacecraft power dissipation, aging or contamination of the thermal control coatings (e.g., insulating blankets, emissive coatings, reflective surfaces, etc), and solar flare events can also induce measurable thermal effects.

WMAP's thermal performance is monitored by a set of platinum resistance thermometers and thermistors (PRTs) which are installed at key locations throughout the system. A representative summary of the instrument's thermal history for the first year of *WMAP* data is presented in Figure 1.4 and Figure 1.8.

1.4.1 Temperature Monitor Architecture

The *WMAP* instrument temperature monitor system is designed to provide high sensitivity thermometry with sensitivity to temperature drifts and resolution of better than 0.25 mK over a temperature range from 40 K to 340 K. Absolute calibration is of secondary importance with a requirement of ± 1 K accuracy. The primary purpose of the temperature monitor system is to permit the removal of any possible instrument or optics temperature driven offset drifts in the radiometers.

The system uses calibrated Rosemount² Platinum Resistance Thermome-

²Rosemount Aerospace, Inc., "Rosemount Model 118MF Platinum Resistance Temperature Sensor," 1989, Eagan, MN, technical specification.

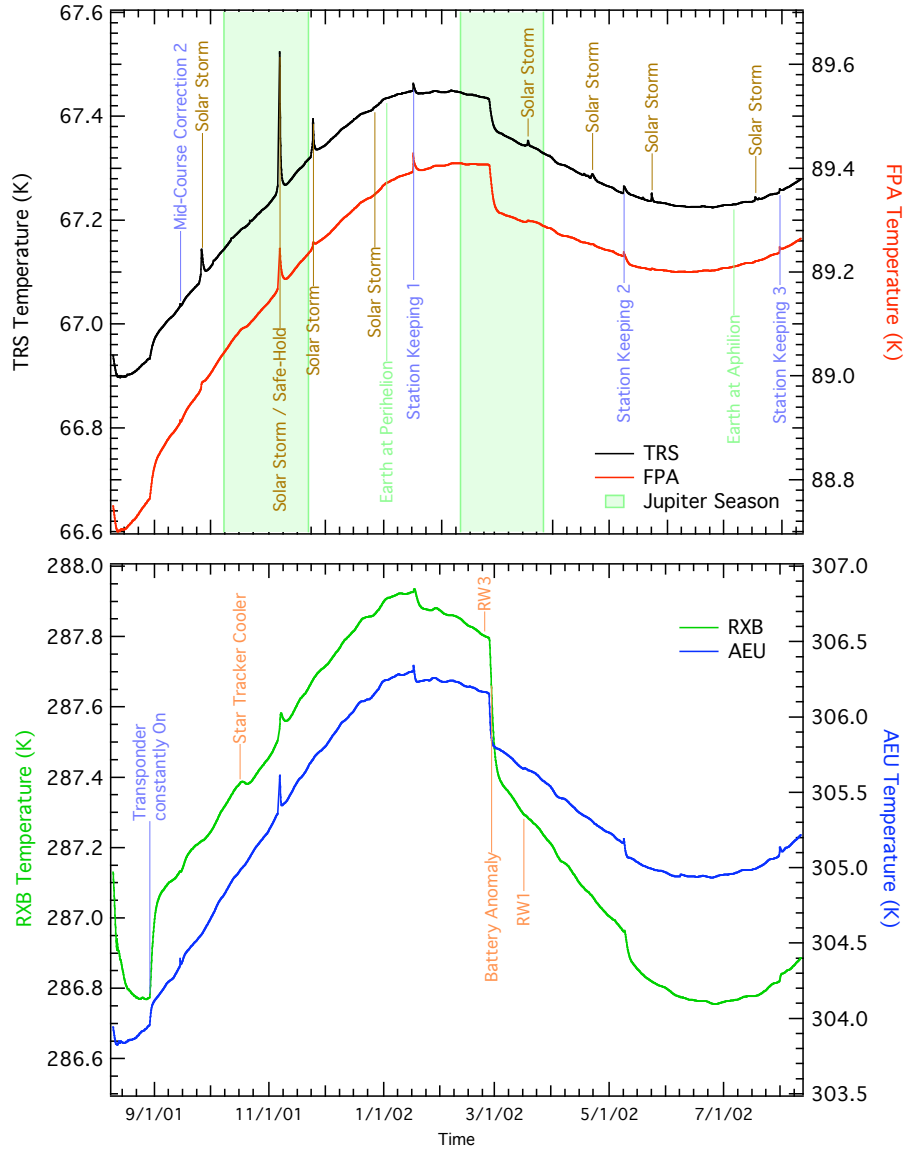


Figure 1.4: First Year Thermal Profile. The measured thermal profile for the first year of operation covers 2001:222 (08/10/2001) to 2002:222 (08/10/2002). Transient events are noted. Modulation from the eccentricity of Earth's orbit is clearly visible. RW1 and RW3 indicate times when there were thermal perturbations due to small changes in reaction wheel drag. See Appendix A for additional details.

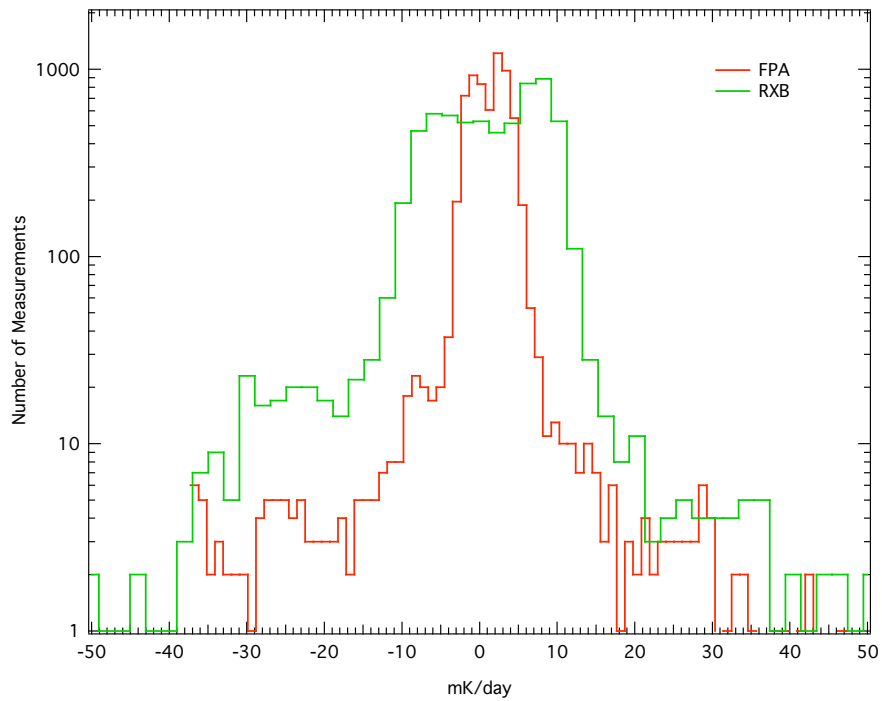


Figure 1.5: Instrument Temperature Rate Histograms. Histograms of the FPA and RXB temperature rates during the first year of science data. The widths of the distributions are 3.9 ± 0.2 mK/day and 11.2 ± 0.6 mK/day for FPA and RXB respectively.

ters (PRTs) energized with a $100 \mu\text{A}$ rms sine-wave current at 195 Hz. The current is driven on a shielded twisted pair of wires of up to 10 m length. A second twisted pair within the same shield carries the voltage on the PRT back to a high-impedance, gain 100 differential receiver. Both the drive current and sense voltage are analog multiplexed with 30 PRTs and 2 calibration resistors per readout card and two cards for a total of 60 PRT circuits. *WMAP* used 57 PRT channels.

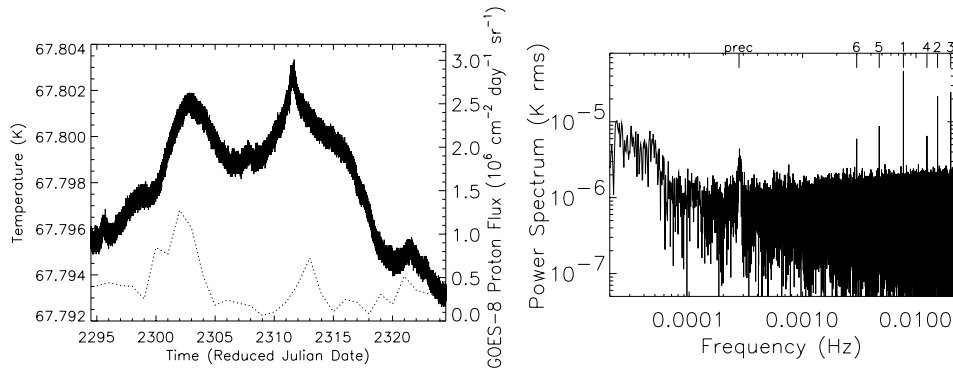


Figure 1.6: PRT Noise Power Spectrum. The left plot is the temperature of the top of the B-side primary mirror for a period of 30 days starting January 20, 2002. The temperature drift is driven by a combination of the changing distance to the sun and solar proton wind. The dotted line is the total solar proton flux as measured by the GOES-8 satellite scaled to the right axis. The right plot is the power spectrum of the temperature over the same period. The low frequency excess is due to the drifts seen on the left. The intrinsic thermometer drift is small relative to the thermal drifts in the system. Special frequencies are marked at the top with labels: “prec” is the spacecraft precession frequency and the numbers indicate the spin frequency harmonic. These are folded back by the Fourier transform. A $45 \mu\text{K}$ RMS signal is seen at the spin harmonic and is the largest spin synchronous temperature signal seen on the spacecraft. The equivalent measurement noise of the thermometer system is about $1 \text{ mK}\sqrt{\text{s}}$.

The PRT sensitivity is approximately $2\Omega/\text{K}$, constant over the range 40 to 360 K. The $100 \mu\text{A}$ excitation gives voltage signal of about $200\mu\text{V}_{\text{RMS}}/\text{K}$. This signal is differenced with a reference sine wave derived from a reference resistor also in the $100 \mu\text{A}$ current loop. The reference voltage amplitude is set with an 8 bit multiplying Digital to Analog Converter (DAC) which nulls the signal to within $\pm 4 \text{ K}$. The 8 nulling bits per PRT are stored in the DEU and set a PRT “window”. The windows overlap by 40%. The differenced signal is AC coupled, amplified and analog synchronously demodulated. The

demodulated voltage is ripple filtered and integrated for 25 195 Hz cycles with a 16 bit synchronous charge-balance V/F ADC. The analog current and voltage sense multiplexers switch between PRTs after the sample integration is complete. Each PRT sample is therefore a 24 bit number including the 8 bits of window information. The gain is set so that the temperature resolution is $125 \mu\text{K}/\text{ADC}$ unit. Each PRT is read once each 23 seconds (i.e., ~ 4 measurements per spin rotation) but not synchronously with the spin.

Assigning a resistance to the digital word for each thermometer sample requires the calibration of the ADC with the window DAC. Because the window DAC has differential non-linearity, the window sizes are not all identical. This leaves jumps in the calculated resistance when switching from one window to another. Because the purpose of the thermometry is largely to monitor temperature variations, these jumps are not important since no window transitions are expected once the temperatures stabilize during the data taking part of the mission. Because the windows overlap by 40%, a transition to the next window starts near the center of the new window minimizing window transitions. The correct window is found either with a binary search at startup, by command or after a saturated ADC samples two times in a row. The binary search is controlled by the DEU. During normal operations, a window transition is initiated when a PRT reading is within 10% of the edge of the current window.

1.4.2 Temperature Monitor Performances

The sensitivity and stability of the temperature monitors is shown in Figure 1.6. Shown is a section of time where the solar input was not changing quickly because the observatory was at the minimum distance from sun and with no large solar flares to drive a thermal disturbance. The sensor shown is mounted to the top of the B-side primary mirror and shows the most thermal variation of any of the sensors. The power spectrum shows low-frequency power from the slow thermal drift of the changing distance to the sun and variations due to solar activity. There is also a $\sim 45 \mu\text{K}$ RMS signal at the spin period of the spacecraft. The equivalent noise power spectral density is $\sim 1 \text{ mK}\sqrt{\text{s}}$ for each of the thermometers.

Temperature calibration of the sensors is derived from the Rosemont calibration curves. Uncorrected offsets in the post-demodulation electronics and differential non-linearity in the window DAC result in an absolute temperature error of $\pm 1 \text{ K}$. The accuracy of temperature variations is derived from reference to precision resistors measured each multiplexing cycle.

Several of the thermal sensors in the FPA assembly exhibit variations which exceed that anticipated from an ideal PRT channel by a factor of several in flight on a time scale of hours. An example of interest is provided by DFW32FPATEET. See Figure 1.7 for power spectrum. In addition to the long-term overall thermal drifts, short-term variations of order 1 mK can be seen in the time order data on this sensor. One observes that this signature is reproduced with smaller amplitude in PRT channels DFW3AOMTT and DFW3BOMTT. This signature is consistent with the presence of a random variation in the physical temperature near this location. From the instrument's thermal parameters, one estimates that this requires a variation in power dissipation $\sim 100\mu W$ in the vicinity of the W3A magic tee.

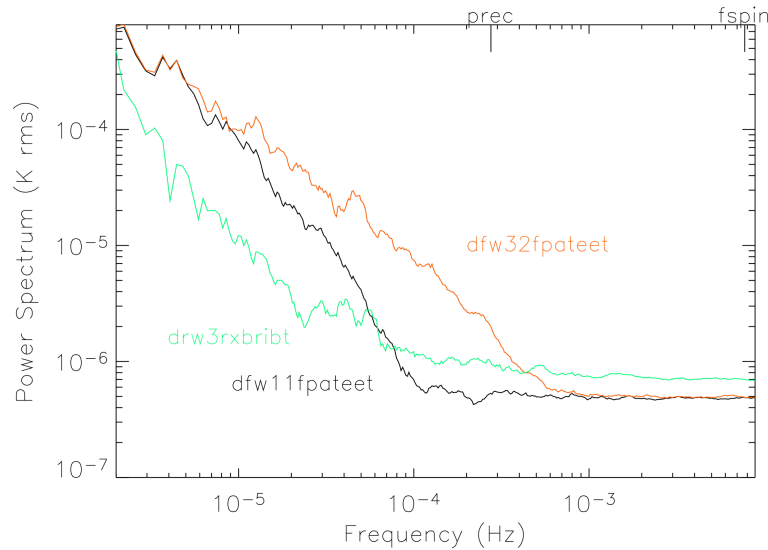


Figure 1.7: FPA and RXB Temperature Power Spectra. PRTs DFW32FPATEET and DFW11FPATEET are mounted on the cold hybrid tees of W32 and W11 radiometers respectively. DRW3RXBRIBT is mounted on an aluminum rib that supports the W3 DA inside the RXB. DFW32FPATEET shows sign of excess thermal variations as described in the text. These power spectra essentially define the envelope of the RXB and FPA temperature stability.

Data from the radiometer outputs and monitors were searched for signals correlated with the variance in DFW32FPATEET temperature sensor. We note that the resolution of the HEMT drain current monitor is sufficient to eliminate the possibility of a bias instability as the primary source of the fluctuations. This effect was not detected in the science data or instrument gain. In addition, the spacecraft housekeeping data were investigated for correlation with on-board activity and the observed effect. The non-detection of a source at the levels investigated suggests that the most likely candidate is a variation in one of the LED bias circuit channels. (note: The LEDs are used to illuminate the HEMT amplifier channel and are operated near saturation.) The fractional variations in the radiometer’s total power monitor, $dT_{sys}/T_{sys} \sim 6 \times 10^{-4}$, dominate over the influence of thermal variations, $dT_{amb}/T_{amb} \sim 1 \times 10^{-5}$. This has a negligible influence on the instrument gain calibration model (Jarosik et al., 2003b). The presence of this noise source at this level has negligible impact upon the quality of the science data.

1.4.3 Sun Driven Yearly Temperature Changes

By design, the spacecraft has a large thermal gradient from its sunlit to dark-side. Temperatures for sensors range from ~ 330 K for objects directly illuminated by the sun to ~ 60 K for elements passively cooled to space. The variation in the satellite’s distance from the sun as it progresses around its orbit at L2 changes the observatory’s average temperature. To estimate the magnitude of this effect we consider the ratio of the solar flux intercepted at the maximum and minimum distance from the sun in the orbit. For a radiatively cooled object in an orbit with numerical eccentricity ε , one finds a relative change in the temperature on the sunlit side of order $dT/T_{amb} \sim \varepsilon \ll 1$. To a good approximation, for the *WMAP* orbit, the eccentricity is equal to that of the Earth, $\varepsilon = 0.017$, yielding an estimated orbital change with temperature of order ~ 5 K for sensors well coupled to objects receiving direct illumination.

Over the course of the first year of observations, for directly illuminated objects, the component of the thermal signature correlated with the satellite-to-solar distance was ~ 4 K. For objects shaded from the sun, the thermal isolation provided for in the design reduces the overall magnitude of this effect. For example, a typical electronics box mounted on the shaded side of the spacecraft hub experienced a temperature correlated with solar distance with amplitude of ~ 1 K. Over the same period of time the thermal reflector system’s temperature, which is shaded from direct solar input and

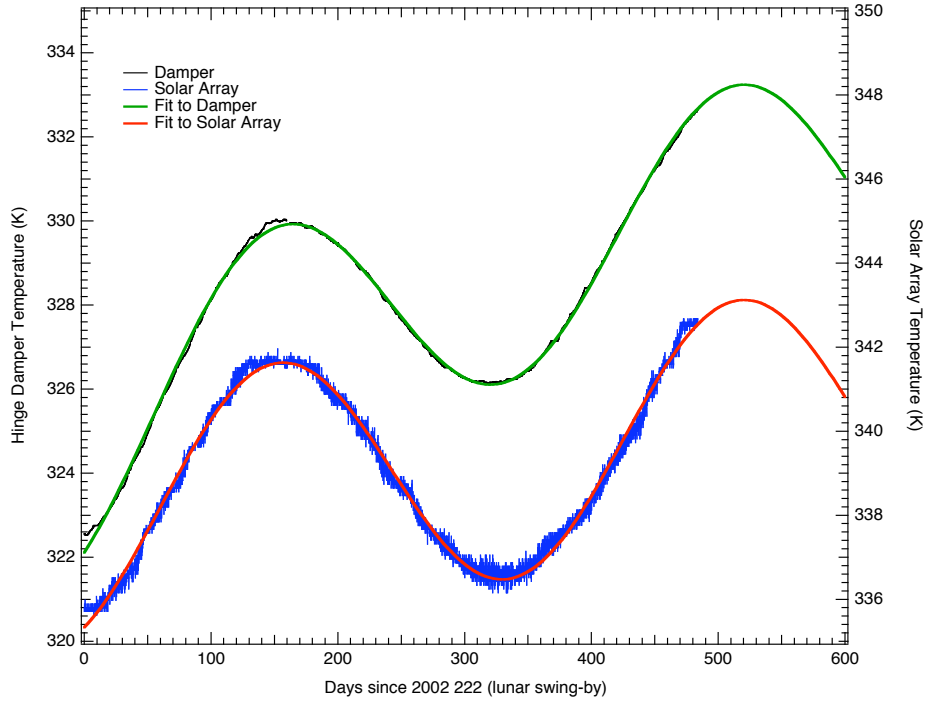


Figure 1.8: Solar Array Temperature Profile. The Damper sensor is mounted on the hinge’s damper of solar array panel 1 while the other is mounted directly on solar panel 2. These two sensors are thermistors and are not part of the instrument’s temperature monitoring system described in section 1.4.1, the excess noise in the solar array sensor is due to the spacecraft temperature readout. Both datasets have been edited to remove spikes induced by the maneuvers and other singular events. Fits to the model described in the text are also displayed.

well thermally tied to the radiator panels, was noted to change by less than ~ 0.2 K. This is consistent with the performance anticipated from a detailed analysis of the thermal design.

1.4.4 Aging of Thermal Control Surfaces

In flight, exposure of the thermal control surfaces to ultraviolet radiation, charged particles, and surface contamination are anticipated to increase solar absorptance while leaving the infrared emittance essentially unchanged (Triolo et al., 1977; Gilmore and Bello, 1994). Published data on the degradation of materials in flight are essentially limited to the more tenuous GEO and LEO environments; however, qualitatively similar trends are anticipated for *WMAP*. Contamination by outgassing of volatile condensable materials, which are subsequently darkened by UV exposure, are anticipated to cause an initial modest increase in the effective aging rate for the first few months to year of the mission. As the outgassing rate tapers off, a slow and monotonic degradation of the coating performance is expected. Such a trend is consistent with the observed thermal performance of the *WMAP* observatory over the first year as presented in Figure 1.8 after taking into account contributions arising from the modest changes in the spacecraft's internal power dissipation.

A simple model of the long term temperature profile of the spacecraft can be written as the product of two terms: a sinusoidal one accounting for the change in temperature due to the L2 motion around the Sun and an exponential one accounting for the change in absorptance due to the degradation of the spacecraft's surfaces. This can be written as

$$T(t) = T_0 \left(1 + \frac{\delta a}{4a_0} \left(1 - e^{-t/\tau} \right) \right) \left(1 + \frac{\delta R}{2R_0} \sin(\omega t + \phi) \right),$$

where T_0 is the initial equilibrium temperature of the spacecraft, a_0 the initial absorptance, δa the change in absorptance over a time large compared to the surface degradation time constant τ , δR is the departure from a circular orbit of radius R_0 and we assume that $\delta a/a_0$ and $\delta R/R_0$ are small compared to unity. Setting ω equal to 2π over 1 year and fitting for all the other parameters we obtain:

Parameter	Damper	Solar Array	
T_{\circ}	324.5	337.9	[K]
$\delta R/R_{\circ}$	-0.017	-0.018	[-]
$\delta a/a_{\circ}$	0.10	0.07	[-]
τ	410	1099	[days]
ϕ	2.16	2.11	[rad]

The value of $\delta R/R_{\circ}$ is in good agreement with Earth’s orbit eccentricity (0.0167) and a 10% change in absorptance is also consistent with previous observations of surface degradation (Gilmore and Bello, 1994).

More accurate determination of the effective aging rates for the thermal control surfaces will be possible as the length of the observational data record is increased. In particular, the observed degeneracy between the time constant for the degradation in the coating performance and an increase in the solar absorptance will be reduced in the second year of operations.

1.4.5 Operationally Induced Disturbances

Control over the spacecraft’s solar absorptance, radiative cooling, and dissipated power density are used to maintain a stable operational temperature for the various components. During nominal operation, changes in the power dissipation in the various electronics boxes have, by design, a negligible impact on the instrument performance. As a rule, as described in Bennett et al. (2003a), passive thermal control is employed for normal observing mode. Survival heaters, which are nominally “off”, are engaged by mechanical thermostats in case of an emergency and the star tracker Peltier coolers which have an internal set point will actively adjust.

Slight changes in *WMAP*’s power dissipation were encountered in maintaining the system. A summary of the instrument’s thermal performance for the first year of operations is presented in Figure 1.4. Several operationally induced disturbances of potential interest from the events log (Appendix A) are indicated. The dominant thermal disturbances in this time frame result from the decision to leave the transponder on and a partial short of a battery cell which subsequently resulted a change in the power system’s nominal voltage. During station keeping maneuvers it is necessary to change in *WMAP*/Sun-line angle. Secondary thermal perturbation sources which occur during these periods include pre-heating the thrusters to operate with approximately optimal and known efficiency, changes in reaction wheel dissipation after momentum unload, and autonomous changes in the power system solar array configuration. Maneuvers and other operationally induced

thermal events which may induce noise in the calibration, are flagged. See Table 1.6.

1.4.6 Radiometric Baselines Discontinuities

During the first year of observations 21 sudden step-like changes in the radiometers outputs were observed. These events have been identified as small changes in the properties of several microwave components resulting from the sudden release of internal stress and are presumably thermally driven. The observed step-like shifts in output are not correlated with changes in HEMT bias. These small steps in radiometer output can be categorized and their point of origin in the system understood by the symmetry of the observed response:

- Waveguide Creep Mode: Differential-mode change in radiometric output (i.e., science signals move with equal and opposite magnitude) induced by slight change in waveguide loss or reflectivity prior to input magic-tee. Signature mimics a small but sudden change in noise temperature.
- Phase Switch Mode: Common-mode step in science output of both radiometer diode readout channels (i.e., science signals move with equal and common magnitude). Can induce second order common mode RF bias. Motion of phase matched waveguide sections could produce similar signatures; however, given the mounting geometry, one anticipates that this would produce relatively slow changes in response rather than producing a sudden step.
- Filter Mode: Step in RF bias of a single diode channel. Signature is consistent with small change total power (i.e., shift in detector diode responsively or band-pass filter bandwidth) after second magic tee.

A typical event is of order ~ 1 mK in amplitude and ones knowledge of the transition time is limited by the data sample rate. In practice, these small events do not cause a discernible change in the DA gain or noise properties. Given the calibration time scale for the system, ~ 1 hour of data on either side of the event is removed, each cut is additionally padded by 1.2 hours on each side by the baseline fitting routine (Hinshaw et al., 2003a). A data loss of $\sim 0.1\%$ is incurred in processing these events. In flight, steps have been observed in radiometer channels W12, W11, Q12, Q11, K11, Ka11 in decreasing order of frequency of event occurrence. Of

the 21 events, 2 affected more than one radiometer channel. The most probable cause of coupling between nearly coincident events is due to the mechanical layout of the radiometer mounting structures. From the band-to-band and channel-to-channel consistency of the maps we conclude that all channels have similar statistical properties after removal of the baseline steps in processing (Hinshaw et al., 2003a).

Cut From yyyy:ddd:hhmm	To yyyy:ddd:hhmm	DA Flag	Notes
2001:223:1800	2001:223:2130	[0,0,1,0,0,0,0,0,0]	Q1 dT glitch
2001:230:1600	2001:230:2010	[0,0,0,0,0,0,1,0,0]	W12 dT glitch
2001:245:1930	2001:246:0110	[0,0,1,0,0,0,0,0,0]	Two close Q1 dT glitches
2001:249:0600	2001:249:1010	[0,0,0,0,0,0,1,0,0]	Small W12 dT glitch
2001:257:1500	2001:258:0900	[1,1,1,1,1,1,1,1,1]	Mid-Course correction #2
2001:282:1700	2001:282:2030	[0,0,0,0,0,0,1,0,0]	Small W12 dT glitch
2001:309:1630	2001:311:0000	[1,1,1,1,1,1,1,1,1]	Solar Storm Induced Safe-hold
2001:316:2300	2001:317:0300	[0,0,1,0,0,0,0,0,0]	Small Q12 dT glitch
2002:013:0810	2002:013:1130	[0,0,0,0,0,0,1,0,0]	W12 dT glitch
2002:016:1500	2002:016:2330	[1,1,1,1,1,1,1,1,1]	Station Keeping #1 (SK1)
2002:053:0500	2002:053:1000	[0,0,0,0,0,0,1,0,0]	W12 dT glitch
2002:053:1700	2002:053:2030	[0,0,0,0,0,0,1,0,0]	W12 dT glitch
2002:057:0200	2002:057:1022	[1,1,1,1,1,1,1,1,1]	Change to VT0
2002:066:2000	2002:067:0000	[0,0,0,0,0,0,1,0,0]	W12 dT glitch
2002:068:2230	2002:069:0200	[0,0,0,0,0,0,1,0,0]	W12 dT glitch
2002:082:2000	2002:082:2300	[0,0,0,0,0,0,1,0,0]	W12 dT glitch
2002:085:0100	2002:085:0400	[0,1,0,0,0,0,0,0,0]	Ka123 RF bias glitch
2002:092:1140	2002:092:1530	[0,0,0,0,0,0,1,0,0]	W12 dT glitch
2002:097:1005	2002:097:1410	[0,1,0,0,0,0,0,0,0]	Ka114 dT and RF bias glitch
2002:100:0600	2002:100:0930	[0,0,0,0,0,0,1,0,0]	W12 dT glitch
2002:100:2210	2002:101:0200	[0,0,0,0,0,0,1,0,0]	W12 dT glitch
2002:123:0200	2002:123:0530	[0,0,0,0,0,0,1,0,0]	W12 dT glitch
2002:128:1400	2002:129:0000	[1,1,1,1,1,1,1,1,1]	Station Keeping #2 (SK2)
2002:211:1456	2002:212:0100	[1,1,1,1,1,1,1,1,1]	Station Keeping #3 (SK3)

Table 1.6: Data Cut Summary. Each line consists of a start time, a stop time and ten element array indicating which DAs are affected, ([1,0,0,0,0,0,0,0,0] = K, [0,1,0,0,0,0,0,0,0] = Ka, etc.). Each cut is additionally padded by 1.2 hours on each side by the baseline fitting routine. Additional cuts are made for Jupiter, Saturn, Mars, Uranus and Neptune if the planet lies within 1.5° radius of a DA's line-of-sight on either the A or the B side.

1.5 The Radiation Environment

1.5.1 Plasma Environment

The Earth's auroral tail is collimated by the solar wind and has a nominal radius of $\sim 20R_E$ at L2. Variations in the solar wind velocity and direction drive fluctuations of the auroral tail from its average position by up to a few tail radii in extent. In an idealized picture, the magnetospheric lobes are relatively small and the magnetosheath has higher density than the lobes but less than the solar wind. Streaming plasma in this region will see essentially open magnetic field lines and it is easier to exhaust out the end than confine the plasma in this region.

To place this in perspective for *WMAP*, we recall the Earth's angular extent as viewed from $\sim 240R_E$ at the L2 halo orbit is in the range of $1^\circ < \theta < 10^\circ$. Based upon these inputs we estimate the major and minor axis of the *WMAP* orbit to be $\sim 4R_E$ and $\sim 40R_E$ respectively. Thus, at L2, the spacecraft will experience the auroral tail, lobes, magnetosheath, and solar wind plasma. In principle, the halo orbit places the satellite inside the magnetosheath for extended periods of time; however, in reality, rotation of Earth's magnetic field and solar wind drive large perturbations from the simple static picture. The surface and internal charge control design described in Bennett et al. (2003a) are compatible with these anticipated environmental conditions.

1.5.2 Spacecraft Charge Control

If the accumulation of charge in an electromagnetic structure exceeds the dissipation rate, a discharge occurs when the critical field strength of the configuration is exceeded. In the space environment, such events can be initiated by sudden changes in electromagnetic field, plasma density, or mechanical stress. The resultant rapid release of electromagnetic energy can induce spurious electrical responses or result in damage to components. In this context, faults in spacecraft performance can result from several basic mechanisms (Frederickson, 1996b,a; Adamo and Matarrese, 1983; Leung et al., 1986; Mizera, 1983).

- Coupling to circuitry increases noise and corrupts desired signal.
- Field strength exceeds dielectric strength and induces mechanical failure.
- Localized heating induces stress which exceeds material strength.

Such discharges can be conducted along wires or ground planes, radiated through free space to a structure that acts as a pick-up antenna, or be directly injected into a circuit. For these reasons, the control of surface and internal charge by proper coating selection, return impedance level, and shielding against electromagnetic and ionizing radiation must be considered for reliable spacecraft operation.

In the case of the *WMAP* observatory, all susceptible circuits are enclosed by an equivalent stopping power of 0.16 cm of aluminum. Grounded lead and copper foils were used to locally augment the available shielding where required in the system. For particularly sensitive subsystems, the signal lines in the harness were filtered or clamped with diode limiters to improve overall immunity. Additional charge control mitigation approaches are outlined in Bennett et al. (2003a).

For the charging environment experienced in the phasing loop portion of the mission *WMAP*, surface discharges can potentially induce electrical transients in the system. Such considerations are of particular interest for elements of the system with a low damage threshold to electrostatic discharge. Charge control objectives were achieved while simultaneously satisfying the thermal design goals by using appropriate dissipative surfaces ($< 10^9 \Omega/\square$) in electrical contact with the spacecraft ground. Materials employed included dissipative paints, indium-tin-oxide films, carbon loaded polymers, thin SiOx coatings on metallic substrates, and conductive tapes. The use of low loss dielectrics exposed to the ambient space plasma in un-illuminated regions is limited to unavoidable patches with area $< 10^{-3}$ of the total surface area. In regions of the spacecraft where photoemission is present, larger dielectric regions can be and are employed. Radiated electromagnetic threats are broadband in nature (Leung and Plamp, 1982; Koons and Chin, 1994) and band-limited by the input waveguide cutoff or input circuitry.

1.5.3 Solar Flares: Charged Particle Heating

Particle heating by the solar wind can produce a small time variable thermal load on the spacecraft (see for example, Jimenez (1988); Vampola et al. (1989)). This effect is a concern when the power deposited by the incident charged particle flux approaches the cooling power available to the system. In practice, this is predominantly a concern for surfaces cooled to low temperatures. Since the *WMAP*'s optics have relatively large thermal mass and operate at a physical temperature around 70 K this is a negligible but measurable effect. In fact, by correlating the GOES-8 proton monitor (<http://sec.noaa.gov/today.html>) with the precision thermal

sensors data from the *WMAP* instrument package, we note that such an effect is observable on the TRS and outer bulk heads of the FPA.

Event Date	$E_p \geq 1\text{MeV}$ p/cm ² sr day	$E_p \geq 10\text{MeV}$ p/cm ² sr day	$E_p \geq 100\text{MeV}$ p/cm ² sr day	Reflectors $\Delta T(\text{mK})$
09/26/01	1.40E+09	2.70E+08	1.80E+06	60
11/06/01	2.40E+09	6.20E+08	3.60E+06	N/A
11/24/01	2.30E+09	3.80E+08	2.00E+05	70
12/27/01	6.80E+07	2.40E+07	6.20E+05	3
03/18/02	2.90E+08	1.90E+06	3.50E+03	12
04/22/02	3.30E+08	1.30E+08	1.20E+06	10
05/23/02	2.60E+08	6.80E+06	2.80E+03	16
07/17/02	2.50E+08	6.40E+06	4.20E+03	8
08/25/02	7.00E+07	6.80E+06	2.10E+04	0
09/07/02	1.00E+08	2.10E+06	3.20E+03	5

Table 1.7: Solar Storms. Major storms encountered by the observatory from launch to the end of the first year data release. The proton data are from the GOES-8 satellite. The spacecraft went into safe-hold mode during the November 6, 2001 solar storm.

As an illustrative example we consider the heating of the *WMAP* primary reflector that occurred during September 26, 2001 solar proton event. This is an example of a severe solar storm with the > 10 MeV proton flux reaching 10^5 times nominal levels. During the event, a thermal change with amplitude $dT \sim 0.06$ K correlated with the event was observed in the primary reflector sensors. From the thermal properties of the TRS in its flight configuration, a change in power loading on the reflector of ~ 6 mW was inferred. One notes for an effective thickness, $dt > 0.5$ mm of aluminum, essentially all incident particles with an energy < 10 MeV, dissipate their energy in the composite structure.

In effect, this portion of the system acts as a bolometric particle detector: the primary reflector serves as an absorber for low energy particles from the solar wind, the PRT is a thermal sensor element, and passive cooling to the sky serves as weak link to the thermal reservoir. A calibration of this bolometric response can be derived from the observed change in temperature which resulted from the removal of RF power to the Z omni antenna (see Appendix A *WMAP* Events Log, 2001:219). The cable which runs through the cavity formed by the back-to-back reflectors on the TRS provides a known ohmic load for calibration. The observed thermal response is consistent with

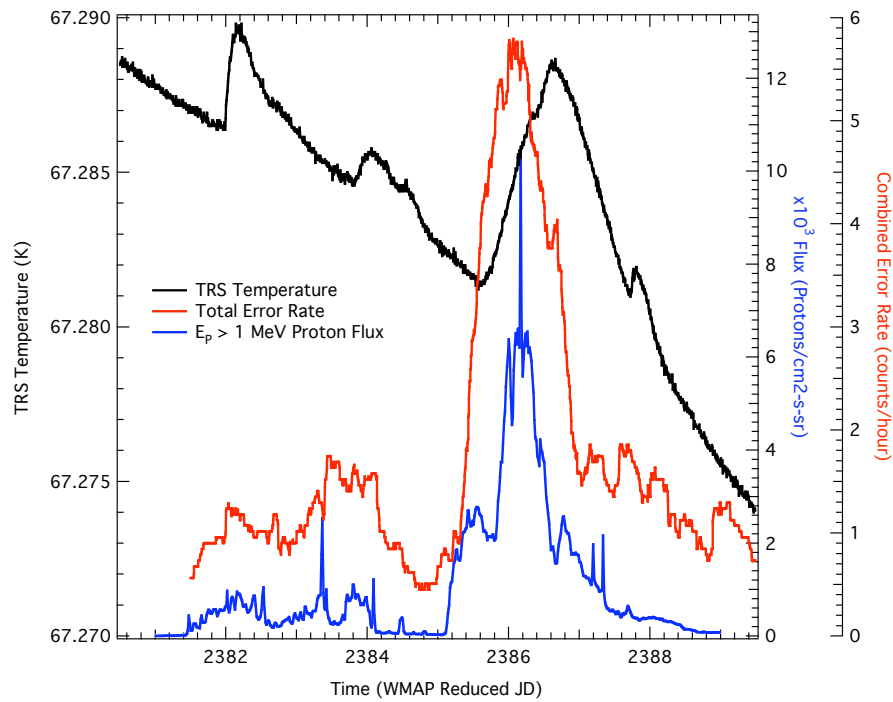


Figure 1.9: Solar Flare Effects on the Observatory. This plot shows the effects of a solar flare (April 17, 2002) on the TRS temperature and on the combined (on-board computer and data recorder) single-bit error rate. The proton data are from the GOES-8 satellite.

the power deposition by the incident particle flux. We conclude that the instrument's observed thermal behavior is consistent with the absorption of an enhanced number of low energy particles encountered during the solar proton event. Given the mm-wave emissivity of the reflector surfaces (Page et al., 2003c), magnitude, and timescale of the thermal response, the resultant differential microwave emission is insufficient to influence the science data.

Chapter 2

Data Pipeline

The pipeline is a set of programs that bring science and housekeeping data from the Science and Mission Operations Center (SMOC) to a set of calibrated full sky maps for each of the 10 *WMAP* differencing assemblies. Numerous additional programs are used to generate ancillary data products such as beam response maps, calibration files and analysis products as well as to permanently archive the data.

A graphical overview of the *WMAP* data processing and analysis pipeline is shown in Figure 2.1. In this chapter we provide a high-level overview of the *WMAP* data pipeline, which is described in details in Hinshaw et al. (2003a).

2.1 Pre-Processing

Raw telemetry data from the satellite is transferred approximately once per day through NASA's Deep Space Network (DSN), to the SMOC, located at the Goddard Space Flight Center. The SMOC monitors the basic health and safety of the Observatory, sends all commands, and requests re-transmissions of data that were missing from a previous transmission. The data are "level-0" processed into a set of time-ordered, daily files that contain science data, instrument housekeeping data, spacecraft data (including attitude and ephemeris data), and event message files. These files are then transferred to the Office of the *MAP* Experiment's General Archive (OMEGA), also at the Goddard Space Flight Center.

Every time a new full day of data arrives in OMEGA, a series of procedures perform the following tasks. 1) Generate a standard set of daily plots that are subsequently visually inspected and archived. 2) Generate a

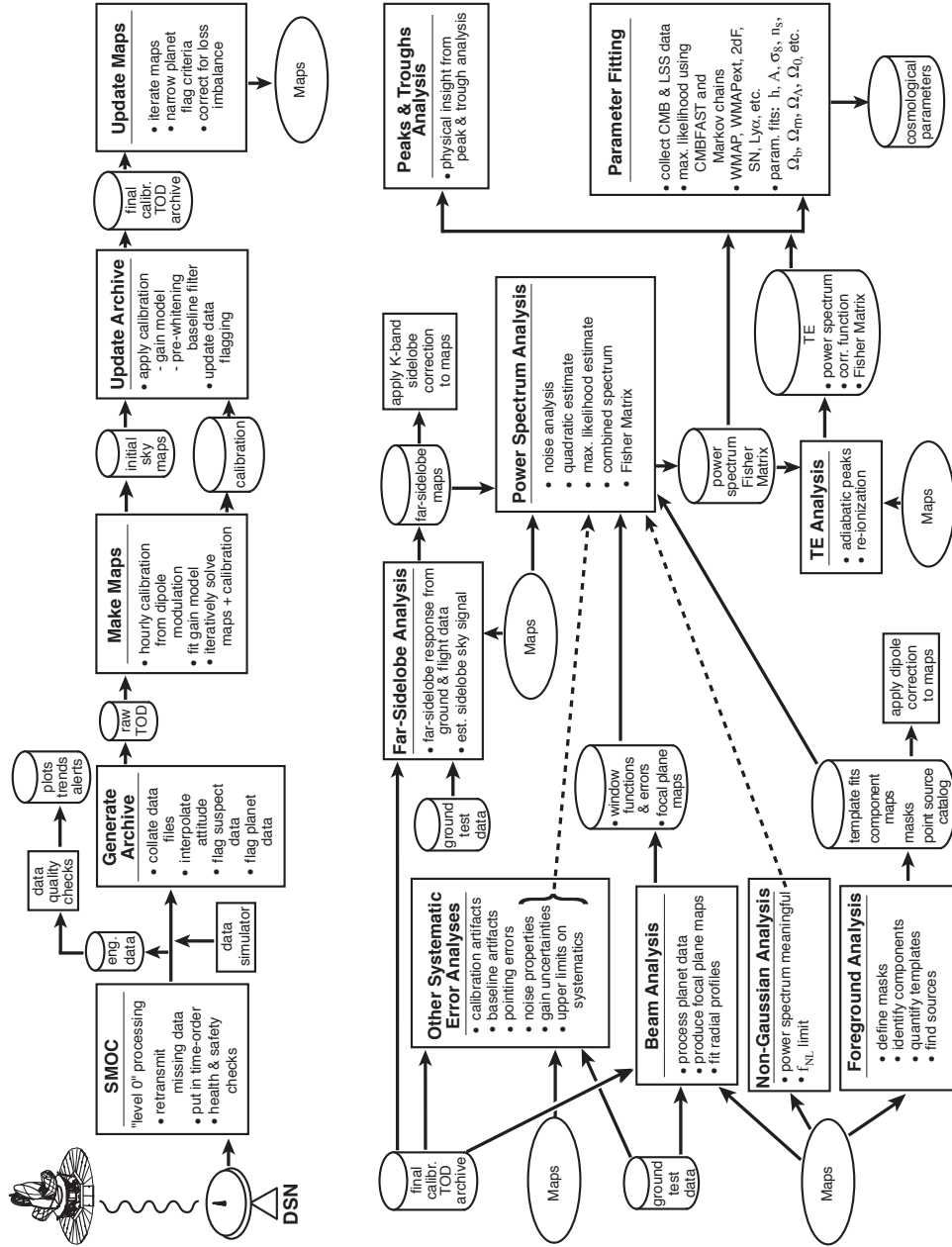


Figure 2.1: An overview of the WMAP pipeline processing flow.

reduced “trending archive” which consists of subsets of the data sampled once every 10 minutes. In the case of the science data, we record the mean and rms of each channel in a 10 minute interval, whereas the housekeeping data are sub-sampled, once per 10 minute interval. 3) Perform a series of data quality checks that search the data for violation of pre-set range limits or excessive time-gradients in the telemetry signals. Limit violations are logged and notification is sent to a member of the science team via e-mail. (Initial limit tests are performed at the SMOC as well.)

At selected time intervals, the level-0 telemetry files are collated by a pre-processor into a master archive of raw (uncalibrated) data. The major functions of the pre-processor are to 1) collate the science and selected housekeeping data into single daily files, 2) flag data that is suspected or known to be unusable, 3) interpolate the attitude and ephemeris data to times that are commensurate with the science data time stamps, and 4) apply a coarse flag to data that is within 7° of one of the outer planets (Mars through Neptune) so that it may be readily rejected from the initial sky maps and readily identified for beam mapping (Page et al., 2003a). (Only Jupiter data is used for making the final beam maps.)

A conservative criterion is employed to define valid data in order to minimize leakage of potential artifacts into the final data set. The thermal sensors on the base plates of various spacecraft electronics are used to monitor the thermal stability after a maneuver. The dominate consideration, although admittedly minuscule in practice, is control over drifts in the baseline. The ~ 16 hour thermal time constant of the FPA, gain model (Jarosik et al., 2003b), and the pre-whitening filter employed on the science data provide a factor of ~ 1000 suppression over small smooth changes in the instruments thermal environment. From simulations of the instrument performance we find that the effect of temperature changes are negligible even before the time they reach a linear gradient. Detailed considerations regarding the effects of thermal drifts on the baseline stability can be found in Hinshaw et al. (2003a).

2.2 Initial Calibration and Map Making

Initial sky maps and calibration data are generated from the raw archive using the iterative map-making algorithm first described in Wright et al. (1996). The initial calibration is determined by fitting the raw time-ordered data to the known signal produced by the CMB dipole. Because the sky signal contains significant higher-order power ($\ell > 1$), the calibration solution

must be iteratively improved in concert with the initial sky map iterations. The convergence of this simultaneous fit has been demonstrated with end-to-end simulations.

The calibration solution converges more rapidly than the sky map does, so we freeze the initial calibration solution after ~ 10 iterations before proceeding to convergence with the sky maps. With the initial dipole-based calibration data in place, a re-processor generates a refined gain and baseline solution and applies this to the data; it also updates the data quality flags as necessary. The re-processor then writes the calibrated data to a new final time-ordered archive. The refinements to the dipole-based gain solution are discussed in Jarosik et al. (2003b). The initial baseline solution is refined using a pre-whitening filter as described in (Wright, 1996).

2.3 Final Sky Map Processing

The final sky maps are computed using the final calibrated time-ordered data as input. The map-making algorithm is fundamentally the same as is used in the initial estimates, but some refinements are added for this final stage of processing. These include:

1. Correcting for a small ($\lesssim 1\%$) loss imbalance between the A and B side sky beams. Jarosik et al. (2003b) demonstrate that this effect is nearly orthogonal to the gain solution, so its inclusion after the calibration processing does not invalidate the gain solution.
2. Weighting individual time-ordered observations by their proper statistical weight to account for the small change in instrument noise ($< 1\%$) over the course of a year due to the 0.9 K seasonal temperature variation (see Figure 1.4 experienced by the instrument cold stage).
3. Computing the planet-boresight angle for each observation at runtime in order to minimize unnecessarily conservative data loss. The criterion used for the first-year maps is a cut of $1^\circ.5$. In the final sky maps, a total of 0.11% of the data was lost to planet avoidance.

The final stage of sky map processing, based on the filtered data, was run for a total of 20 iterations. Convergence was determined by measuring the rms difference between pairs of iterations for a given differencing assembly. For example, the difference between the 10th and 20th iteration of the W2 sky map is $0.08 \mu\text{K}$ rms. We estimate that artifacts due to lack of solution

convergence are less than $0.1 \mu\text{K}$ rms with all of the power being in the low multipoles, $\ell < 10$.

Chapter 3

Data Products

Each section of this chapter contains the description of a particular delivered data product and contain at least the following information:

- Description of the data
- Data format
- Quick summary of the methodology use to obtain the data set
- References to papers describing the more technical details.

The time-ordered data are described in Chapter 4. More information on how to read both maps and time-ordered data are contained in Chapter 5 and in Appendix B. All the data can be downloaded at:

<http://lambda.gsfc.nasa.gov/>

3.1 Calibrated Sky Maps

3.1.1 I Maps (Individual Differencing Assemblies)

Coord System	Galactic
Projection Type	HEALPix Nested
Res/N_{side}	9/512
N_{pix}	3145728
Resolution	0.23° – 0.93° (frequency dependent)
Units	mK (Thermodynamic)
Format	FITS
# of Files	10

Iterative algorithms are used to create skymaps from the calibrated differential time-ordered *WMAP* data for each of the ten differencing assemblies. Each pixel in a map represents a sky temperature for the bandpass appropriate to the differencing assembly. The CMB dipole has been removed and the zero point of each map has been set using a Galactic $\csc(|b|)$ model (see Bennett et al. (2003c)).

The data provided in each map consist of two fields for each pixel:

- Thermodynamic temperature, in mK
- Effective number of observations, N_{obs}

Pixel noise can be evaluated from N_{obs} via $\sigma = \sigma_o / \sqrt{N_{obs}}$, where σ_o for each differencing assembly is listed in the following table:

DA	σ_o [mK]	DA	σ_o [mK]
K1	1.42366	V2	2.93683
Ka1	1.44883	W1	5.85196
Q1	2.26677	W2	6.53276
Q2	2.15567	W3	6.88032
V1	3.28789	W4	6.72537

More details can be found in:

HINSHAW, G. F. ET AL., 2003a. “First Year Wilkinson Microwave Anisotropy Probe (*WMAP*) Observations: Data Processing and Systematic Error Limits”. *ApJ* Submitted

WRIGHT, E. L., HINSHAW, G., AND BENNETT, C. L., 1996. “Producing Megapixel Cosmic Microwave Background from Differential Radiometer Data”. *ApJ* **458**:L53

3.1.2 I Maps (Per Frequency)

Coord System	Galactic
Projection Type	HEALPix Nested
Res/N_{side}	9/512
N_{pix}	3145728
Resolution	$0.23^\circ - 0.93^\circ$ (frequency dependent)
Units	mK (Thermodynamic)
Format	FITS
# of Files	5

Five maps, one for each of the five frequency bandpasses observed by *WMAP*. These frequency maps are derived from the individual differencing assembly maps.

For each pixel in a frequency map, noise weighting is used to compute the average temperature from the individual differencing assembly map values. Since there is only one differencing assembly for the K and Ka bandpasses, the K and Ka frequency maps are identical to the K1 and Ka1 differencing assembly maps. The Q map is the noise-weighted result from combining Q1 and Q2, V is derived from V1 and V2, and W is made from W1, W2, W3 and W4.

The data provided in each frequency map consist of two fields for each pixel:

- Thermodynamic temperature, in mK
- Effective number of observations, N_{obs}

Pixel noise can be evaluated from N_{obs} via $\sigma = \sigma_o / \sqrt{N_{obs}}$, where σ_o (in mK) for each frequency is listed in the following table:

DA	σ_o [mK]
K	1.42366
Ka	1.44883
Q	2.21122
V	3.11236
W	6.49760

3.1.3 Smoothed I Maps (Per Frequency)

Coord System	Galactic
Projection Type	HEALPix Nested
Res/N_{side}	9/512
N_{pix}	3145728
Resolution	1°
Units	mK (Thermodynamic)
Format	FITS
# of Files	5

These maps result from smoothing the I Maps (per frequency) to a common resolution of 1 degree. Smoothing is performed in Fourier space by transforming the map to a_{lm} 's, up to the Nyquist frequency of the map, applying a window function determined by the smoothing kernel, then transforming back to pixel space. The smoothing window function is computed from the ratio of the desired output 1 degree FWHM Gaussian window function and the beam window function appropriate to each *WMAP* frequency bandpass.

Note that the instrument noise and sky signal are correlated between neighboring pixels in these maps. These maps are not intended for use in CMB studies, but rather for cases such as foreground analysis where a common resolution among maps is useful.

Pixel temperatures are provided in thermodynamic units, in mK. Because of the difficulty in associating a noise with each pixel, the effective number of observations (N_{obs}) has been set to 1.0 for all pixels.

3.2 Derived CMB Products

3.2.1 TT Cross-Power Spectra

Units	μK^2
Format	ASCII
# of Files	28

A cross-power spectrum is an angular power spectrum computed using the quadratic estimator on maps from two different differencing assemblies. Since the noise between the two different maps is uncorrelated, an unbiased estimate of the underlying power spectrum is achieved.

In order to minimize contamination from foregrounds signals, a Galactic foreground model was subtracted from the maps prior to computing the cross-power spectra, and a masking cut applied to high intensity regions of the Galactic plane. The foreground model was computed using a linear combination of map templates representing synchrotron, free-free, and dust components.

Cross-power spectra obtained from all 28 combinations of the 8 differencing assemblies Q1-W4 are presented. These 28 cross-power spectra form the basis of the *WMAP* combined TT power spectrum, which is the best estimate power spectrum.

The data product file, in FITS format, contains 28 binary table extensions, one for each of the 28 cross-power spectra. Each extension is named according to the differencing assembly combination used for that spectrum. Cross-power spectra are in units of μK^2 .

More details can be found in:

HINSHAW, G. F. ET AL., 2003b. “First Year Wilkinson Microwave Anisotropy Probe (*WMAP*) Observations: The Angular Power Spectrum”. *ApJ* Submitted

BENNETT, C. L. ET AL., 2003c. “First Year Wilkinson Microwave Anisotropy Probe (*WMAP*) Observations: Foreground Emission”. *ApJ* Submitted

3.2.2 Combined TT Power Spectrum

Units μK^2
Format ASCII
of Files 1

The best-estimate *WMAP* power spectrum of the CMB is produced from a weighted combination of the 28 cross-power spectra. For multipole moment $\ell < 100$, the combined spectrum is formed from a simple weighted average of the fifteen V- and W-band cross-power spectra. For $\ell > 100$, all 28 cross-power spectra are used to form the combined spectrum, but different weighting schemes are used for the three separate ℓ regimes.

The TT power spectrum data are provided as a table containing the following three columns:

- Multipole moment ℓ
- Power spectrum in units of μK^2
- Corresponding diagonal elements of the Fisher matrix

The diagonal elements provide a crude estimate of the error, but should not be used as exact error bars. The complete Fisher matrix should be used for that purpose.

More details can be found in:

HINSHAW, G. F. ET AL., 2003b. “First Year Wilkinson Microwave Anisotropy Probe (*WMAP*) Observations: The Angular Power Spectrum”. *ApJ* Submitted

VERDE, L. ET AL., 2003. “First Year Wilkinson Microwave Anisotropy Probe (*WMAP*) Observations: Parameter Estimation Methodology”. *ApJ* Submitted

3.2.3 TE Power Spectrum

Units μK^2
Format ASCII
of Files 2

The angular power spectrum of the temperature-polarization correlations is computed using a quadratic estimator. C_ℓ^{TE} is computed individually for each *WMAP* frequency band, using uniform weight for the temperature map and noise weight for the polarization maps. The power spectra are then combined using noise-weighted QVW data for $\ell > 21$ where foregrounds are insignificant, and a fit to CMB plus foregrounds using all five frequency bands for $\ell \leq 21$.

The TE power spectrum data are provided as a table containing the following three columns:

- Multipole moment ℓ
- Power spectrum in units of μK^2
- Corresponding diagonal elements of the Fisher matrix

The diagonal elements provide a crude estimate of the error, but should not be used as exact error bars. The complete Fisher matrix should be used for that purpose.

More details can be found in:

KOGUT, A. ET AL., 2003. "First Year Wilkinson Microwave Anisotropy Probe (*WMAP*) Observations: TE Polarization". *ApJ* Submitted

3.2.4 Likelihood Code

Format FORTRAN 90

of Files 1

Proper assignment of errors to points in the CMB angular power spectra requires the use of a Fisher matrix. Since some components that go into making the Fisher matrix are model dependent, we provide FORTRAN 90 code which, given an input CMB model power spectrum, will compute the likelihood of that model fit to WMAP data and optionally return the inverse Fisher matrix.

More details can be found in:

HINSHAW, G. F. ET AL., 2003b. “First Year Wilkinson Microwave Anisotropy Probe (WMAP) Observations: The Angular Power Spectrum”. *ApJ* Submitted

VERDE, L. ET AL., 2003. “First Year Wilkinson Microwave Anisotropy Probe (WMAP) Observations: Parameter Estimation Methodology”. *ApJ* Submitted

3.3 Derived Foreground Products

3.3.1 Internal Linear Combination Map

Coord System	Galactic
Projection Type	HEALPix Nested
Res/N_{side}	9/512
N_{pix}	3145728
Resolution	1°
Units	mK (Thermodynamic)
Format	FITS
# of Files	1

The Internal Linear Combination (ILC) map is formed from a weighted linear combination of the 5 smoothed I maps in which the weights are chosen to maintain the CMB anisotropy signal while minimizing the Galactic foreground contribution. The weights are determined by minimizing the variance of the measured temperatures with the additional constraint that sum of the weights is equal to 1. To account for the spatial variation of the spectral indices of the various foreground components across the sky and in particular in the Galactic plane, the sky is divided into 12 regions: 11 regions within the inner Galactic plane and 1 covering the outer Galactic plane and high Galactic latitudes. The weights are calculated for each of the 12 regions and the final ILC map is generated using the obtained coefficients after smoothing the region boundaries with a 1.5° kernel. Pixel temperatures are in given in mK (thermodynamic).

The ILC map is useful for visual presentation of the CMB anisotropy signature and for foreground studies. However, because of the complex noise properties of this map, it should **NOT** be used for CMB studies.

More details can be found in:

BENNETT, C. L. ET AL., 2003c. “First Year Wilkinson Microwave Anisotropy Probe (WMAP) Observations: Foreground Emission”. *ApJ* Submitted

3.3.2 Foregrounds Derived from Maximum Entropy Method

This description applies to any of the three foregrounds recovered using the Maximum Entropy Method: synchrotron, free-free and dust.

Coord System	Galactic
Projection Type	HEALPix Nested
Res/N_{side}	8/256
N_{pix}	786432
Resolution	1°
Units	mK (Antenna)
Format	FITS
# of Files	5

The Maximum Entropy Method (MEM) is used to derive all-sky maps of the synchrotron, free-free and dust foregrounds at each of the 5 *WMAP* frequencies. Using the smoothed I maps minus the ILC map as input, simple power law representations of each of the foregrounds are fit to each pixel independently. The synchrotron spectral index is allowed to vary for each pixel, while the free-free and dust spectral indices are assumed to be constant over the sky. The MEM technique fits for the separate components by maximizing an entropy functional using the listed templates as priors:

Component	Prior
Synchrotron	408 GHz Haslam Map
Free-Free	H α Map
Dust	FDS Map

The three model foregrounds are provided in separate files for each of the five *WMAP* frequencies. Note that the model temperatures are in mK, antenna temperature, rather than in thermodynamic units.

More details can be found in:

BENNETT, C. L. ET AL., 2003c. “First Year Wilkinson Microwave Anisotropy Probe (*WMAP*) Observations: Foreground Emission”. *ApJ* Submitted

3.3.3 Point Source Catalog

Format ASCII

of Files 1

This is a catalog of 208 point sources detected in the *WMAP* sky maps independently from any previous surveys. The sources listed in the catalog were detected as ≥ 5 sigma peaks in *WMAP* maps that have been weighted by the square root of the number of observations and optimally filtered for point source detection. The position of each source is obtained by fitting a Gaussian profile plus a baseline to each detected peak. Of the 208 detected sources, 203 have one or more known counterparts; the 5 sources that do not are very close to the detection threshold and are thought to be spurious. The catalog lists the following parameters for each source:

- Position
- Brightness in the 5 *WMAP* bands
- Spectral index
- Counterpart (if known)

More details can be found in:

BENNETT, C. L. ET AL., 2003c. “First Year Wilkinson Microwave Anisotropy Probe (*WMAP*) Observations: Foreground Emission”. *ApJ* Submitted

3.4 Ancillary Data

3.4.1 Intensity Mask

Coord System	Galactic
Projection Type	HEALPix Nested
Res/N_{side}	9/512
N_{pix}	3145728
Resolution	N/A
Units	N/A
Format	FITS
# of Files	3

A number of *WMAP* data analysis applications have been aided by the use of pixel intensity masks which exclude “bright” portions of the sky from use. These masks were used in the generation of maps and CMB angular power spectra. The 3 masks provided allow for the selective exclusion of portions of the sky at different flux levels. The masks are based on the K-band map and include a 0.6 degree radius exclusion area around known point sources.

Mask	% of pix cut including sources
Kp0	23.2
Kp2	15.0
Kp12	5.8

Mask values for each map pixel are provided in the N_{obs} field of the data file (the ‘Temperature’ field is set to zero for all pixels and not used). A mask value of zero means that the pixel is excluded; a value of 1 means that the pixel is accepted.

More details can be found in:

BENNETT, C. L. ET AL., 2003c. “First Year Wilkinson Microwave Anisotropy Probe (*WMAP*) Observations: Foreground Emission”. *ApJ* Submitted

3.4.2 Far-Sidelobe Maps

Coord System	Spacecraft
Projection Type	HEALPix Nested
Res/N_{side}	7/128
N_{pix}	196608
Resolution	N/A
Units	[-]
Format	FITS
# of Files	10

Low resolution maps of the antenna gain response over 4π steradians for each of the 10 *WMAP* detector assemblies. While *WMAP*'s optical system gain drops very rapidly when moving away from the main beam line-of-sight, the emission of the extended Galactic foreground can be 1000 times brighter than the fluctuations of the CMB and can cover very large solid angles. It is therefore extremely important to fully characterize the antenna gain response. The Far-Sidelobe Maps are based on compilations of data from the following sources:

- GSFC anechoic chamber antenna range
- Princeton outdoor antenna range
- In flight lunar data
- Physical optics code theoretical predictions

The gain pattern is presented in spacecraft coordinates, such that the X axis is parallel to the plane of the radiators, -Z is the anti-sun direction of the spin axis, and Y is perpendicular to both. The gain, $4\pi/\Omega^S$, is relative to isotropic in dimensionless units where Ω^S is the symmetrized beam solid angle. Positive values refer to A-side pickup, and negative values to B-side pickup.

More details can be found in:

BARNES, C. ET AL., 2003. "First Year Wilkinson Microwave Anisotropy Probe (*WMAP*) Observations: Characterization of the Far-Sidelobes". *ApJ* Submitted

3.4.3 Beam Maps

Coord System	Focal Plane
Projection Type	Rectilinear, pixelized at 2.4'(0.04°)
Resolution	0.23° – 0.93° (frequency dependent)
Units	mK (Thermodynamic)
Format	FITS
# of Files	1

The main and near-sidelobe response of each of the 20 *WMAP* antenna feeds has been mapped in-flight using observations of Jupiter. These maps are constructed from calibrated time-ordered observations in which Jupiter passed within 5° of either the A- or B-side *WMAP* optic axis, using data from Nov/Dec 2001 and Feb/Mar 2002. The time-ordered observations are corrected to a fiducial Jupiter distance of 5.2 AU, background subtracted and corrected for aberration. For purposes of constructing beam maps, the observations are assigned to 2.4 arcminute bins on a coordinate grid centered on either the A or B-side focal plane. The beam response for each feed is computed from the average temperature in each bin. No correction has been made for the side-A vs. side-B input transmission imbalance.

Beam maps are provided in 10 FITS image format files, one file for each differencing assembly. Each file contains:

- Beam maps for the A and B sides, in mK (antenna temperature)
- Statistical errors of each bin of the A and B sides beam maps, in mK (antenna temperature). The statistical error are based on the number of observations in each bin.

The beam coordinates form an equal area rectangular coordinate system centered on the optic axis of the spacecraft. They are related to coordinates θ (elevation from optic axis) and ϕ (azimuth about optic axis) as follows:

$$X_{beam} = 2 \sin(\theta/2) \cos(\phi)$$

$$Y_{beam} = 2 \sin(\theta/2) \sin(\phi).$$

More details can be found in:

PAGE, L. ET AL., 2003a. “First Year Wilkinson Microwave Anisotropy Probe (*WMAP*) Observations: Beam Profiles and Window Functions”. *ApJ* Submitted

3.4.4 Beam Transfer Functions

Units see text
Format ASCII
of Files 10

Window functions appropriate to each of the ten *WMAP* detector assemblies have been derived in-flight from the calibrated time-ordered observations of Jupiter. For each detector assembly, a symmetrized radial beam profile is computed by fitting the ensemble of individual A- and B-side Jupiter observations with Hermite polynomials of even order. The beam transfer function is then computed from the Legendre transform of the fitted radial beam profile. The window function applicable to power spectra is the square of the beam transfer function.

Window functions are presented as ASCII tables, with the first column being multipole moment ℓ and the second column the window function (amplitude) normalized to 1.0 at $\ell = 1$.

More details can be found in:

PAGE, L. ET AL., 2003a. “First Year Wilkinson Microwave Anisotropy Probe (*WMAP*) Observations: Beam Profiles and Window Functions”. *ApJ* Submitted

HINSHAW, G. F. ET AL., 2003b. “First Year Wilkinson Microwave Anisotropy Probe (*WMAP*) Observations: The Angular Power Spectrum”. *ApJ* Submitted

Chapter 4

Time Ordered Data (TOD)

WMAP's Telemetry data consists of many packet types; each packet type contains several measurements with some sort of common theme. Once on the ground and delivered to the data analysis facility, these packets are sorted and a subset are combined into records spanning 46.08 seconds; these records comprise the time-ordered data (TOD) archive. This archive is maintained in a collection of files, each spanning one day of data.

The TOD archive is distributed to the public through daily files written using the Flexible Image Transport Standard (FITS) format. Each file is broken up into a collection of five binary FITS tables:

1. Meta Data Table
2. Science Data Table
3. Analog Instrument Housekeeping Data Table
4. Digital Instrument Housekeeping Data Table
5. Line-Of-Sight Data Table

In four of the five tables, each row has a time associated with it. This time is reported in a modified reduced Julian day format. Packet times require precision to better than one tenth of a millisecond, so in order to retain sufficient precision in the numerical representation of the time, it is necessary to modify the definition of the reduced Julian day. To convert a modified reduced Julian day to a Julian day, add 2,450,000 to it.

A discussion of each table, followed by a very brief discussion of FITS headers, follows. In these discussions, records refer to TOD records and

packets refer to the telemetry packets received from *WMAP*. The science data is transmitted in two packets; these are combined into a single data structure called major science frames.

4.1 The Meta Data Table

The meta data table contains general information describing each record in the time ordered data archive for that day. Each row corresponds to one 46.08 second record; each column represents:

Name	Description
TIME	The time of the start of the record, represented as a modified reduced Julian day.
POSITION	A three element Cartesian vector supplying the position (in kilometers) of <i>WMAP</i> at the start of the record. It is measured from the Sun with the +X axis in the J2000 0hr right ascension direction and the +Z axis in the J2000 +90deg. declination direction.
VELOCITY	A three element Cartesian vector supplying the velocity (in km/sec) of <i>WMAP</i> at the start of the record, using the same coordinate system as the POSITION vector.
GEOPOS	A three element Cartesian vector supplying the position (in kilometers) of <i>WMAP</i> at the start of the record. It is measured in the same coordinate system as the POSITION vector, centered on the Earth instead of the Sun.
GEOVEL	A three element Cartesian vector supplying the velocity (in km/sec) of <i>WMAP</i> at the start of the record, using the same coordinate system as the GEOPOS vector.
QUATERN	A 4×33 array containing a four element quaternion for the start of each major science frame plus one for the preceding science frame and one for each of the two following science frames.
NSCI	The number of major science frames in the record. There will generally be thirty [the maximum number of frames allowed in a record].
NDIHK	The number of digital instrument housekeeping packets there are in the record.

4.2 The Science Data Table

The science data table contains the major science frames recorded for that day. Each frame consists of two science data telemetry packets that have been combined into a single data structure.

A single TOD record contains thirty 1.536 second major science frames. The data has been calibrated and are reported in millikelvin. Each row corresponds to one frame; each column represents:

Name	Description
TIME	The time of the start of the science frame, represented as a modified reduced Julian day.
K1	The K-band differencing assembly array.
KA1	The KA-band differencing assembly array.
Q1	The first Q-band differencing assembly array.
Q2	The second Q-band differencing assembly array.
V1	The first V-band differencing assembly array.
V2	The second V-band differencing assembly array.
W1	The first W-band differencing assembly array.
W2	The second W-band differencing assembly array.
W3	The third W-band differencing assembly array.
W4	The fourth W-band differencing assembly array.
GenFlags	A set of bit-coded quality flags describing the entire science frame [the general flags].
DAFlags	An array of ten sets of bit-coded quality flags, each describing one differencing assembly.
Error1	A two bit-coded error code transmitted by <i>WMAP</i> describing the science frame. There are two—one for each science telemetry packet.
Error2	A bit-coded error code transmitted by <i>WMAP</i> describing the science frame. There are two—one for each science telemetry packet.
FrmInd	The index within the day of the time-ordered data record containing this science frame.
SciInd	The index of the science frame within its time-ordered data record.

Each differencing assembly (DA) array consists of four channels measured N times where N depends upon the bandpass. For the first data release, however polarization data are not available and the four channels

are averaged together,¹ so each differencing assembly array consists of N measurements. N for each bandpass is:

K	Ka	Q	V	W
12	12	15	20	30

The bit-coded quality flags are set during processing. These flags are:

General Flags

- Bit 0 There is a problem with the spacecraft attitude for this science frame.
- Bit 1 A filler telemetry packet (science, instrument, or spacecraft) affects this science frame. A filler packet is an empty frame that replaces a missing packet.
- Bit 2 The transmitter is on. Since the transmitter is now always on this flag will not be implemented.
- Bit 3 *WMAP* is not in observing mode.
- Bit 4 There is no science data in this frame. Not implemented.
- Bit 5 The sun is visible over the sun shield. In other words, the angle between the sun and the +Z axis is greater than some angle (see programs.pars for the shield angle).
- Bit 6 The Earth is visible over the sun shield. In other words, the angle between the Earth and the +Z axis is greater than some angle (see programs.pars for the shield angle).
- Bit 7 The moon is visible over the sun shield. In other words, the angle between the moon and the +Z axis is greater than some angle (see programs.pars for the shield angle).

DA Specific Flags

- Bit 0 This flag indicates that the data in the frame is suspect. An ASCII log file is used to flag time ranges that contain suspect data.
- Bit 1 Mars is visible in the A-side beam.
- Bit 2 Mars is visible in the B-side beam.
- Bit 3 Jupiter is visible in the A-side beam.

¹The IDL procedure `pckt2mnemonic` (see section 5.2) provided with the *WMAP* software package is designed to be compatible with future data releases and will accept as input any of the four channels but will always return the same average value.

- Bit 4 Jupiter is visible in the B-side beam.
- Bit 5 Saturn is visible in the A-side beam.
- Bit 6 Saturn is visible in the B-side beam.
- Bit 7 Uranus is visible in the A-side beam.
- Bit 8 Uranus is visible in the B-side beam.
- Bit 9 Neptune is visible in the A-side beam.
- Bit 10 Neptune is visible in the B-side beam.

Finally, the bit-coded error codes in the science telemetry packets shown below are extracted from the internal *WMAP* document: “*MAP DEU Flight Command and Telemetry Packets Definition*,” by Carlos Trujillo of NASA/GSFC.

Error 1

- Bit 0 Unused.
- Bit 1 Band Buffer Overflow. The memory location where the pointer to the next available storage location inside the Band buffer has been corrupted. In order to avoid writing science data outside the boundaries of the Band buffer, this check is performed prior to storage of the next 40 science data samples into the Band buffer. A detected overflow condition is handled by not storing science data into the Band buffer. Correction of this error is done during science data packetization (the pointer value is cleared as part of cleaning operations).
- Bit 2 K Band Accumulation Buffer Overflow. The memory location where the pointer to the next available storage location for the K Band Accumulation buffer has been corrupted. In order to avoid writing science data outside the boundaries of this buffer, this check is performed prior to calculation of the next K Band accumulated result. If the overflow condition is detected, accumulation data will not be processed nor stored.

Bit 3	Ka Band Accumulation Buffer Overflow. The memory location where the pointer to the next available storage location for the Ka Band Accumulation buffer has been corrupted. In order to avoid writing science data outside the boundaries of this buffer, this check is performed prior to calculation of the next Ka Band accumulated result. If the overflow condition is detected, accumulation data will not be processed nor stored.
Bit 4	Q Band Accumulation Buffer Overflow. The memory location where the pointer to the next available storage location for the Q Band Accumulation buffer has been corrupted. In order to avoid writing science data outside the boundaries of this buffer, this check is performed prior to calculation of the next Q Band accumulated result. If the overflow condition is detected, accumulation data will not be processed nor stored.
Bit 5	V Band Accumulation Buffer Overflow. The memory location where the pointer to the next available storage location for the V Band Accumulation buffer has been corrupted. In order to avoid writing science data outside the boundaries of this buffer, this check is performed prior to calculation of the next V Band accumulated result. If the overflow condition is detected, accumulation data will not be processed nor stored.
Bit 6	W Band Accumulation Buffer Overflow. The memory location where the pointer to the next available storage location for the W Band Accumulation buffer has been corrupted. In order to avoid writing science data outside the boundaries of this buffer, this check is performed prior to calculation of the next W Band accumulated result. If the overflow condition is detected, accumulation data will not be processed nor stored.

Bit 7 Science Pointers Out of Spec - The values for all the storage and retrieval pointers for Band and Accumulation buffers are examined at the end of each Science Data Cycle. The FSW can be fooled into believing that a Science Data Cycle ended (corruption of Timing.SciDataCycles counter) and attempt an early packetization of the science data. This attempt will be accepted, but the condition is flagged. Clearing all science data cycle counters and pointers (therefore correcting any corrupted memory locations) recovers from this error.

Error 2

Bits 1–15 Non-matching channel address counter - For each science data sample collected from the AEU the actual reported address of the sample (0 through 39) is verified against the address value requested by the FSW. Any non-matching address values will void the science data sample collected and a value of 0 will be stored in the expected Band buffer location.

4.3 The Analog Instrument Housekeeping (AIHK) Data Table

The AIHK data table contains the AIHK packets recorded for that day. This data represents physical measurements [such as temperatures, voltages, and currents] of the instrument indicating its current state.

A single TOD record contains one AIHK telemetry packet consisting of two 23.04 second sweeps. Each row in the table corresponds to one sweep; each column represents:

Name	Description
TIME	The time of the start of the telemetry packet, represented as a modified reduced Julian day. This time will be reported twice in the table—once for each sweep extracted from an AIHK packet.
PDU	The Power Distribution Unit (PDU) data block of 97 elements.
AEU1	The Analog Electronics Unit (AEU) #1 data block of 57 elements.
AEU2	The Analog Electronics Unit (AEU) #2 data block of 57 elements.
AWIN1	The 16 element window range block corresponding to AEU1.
AWIN2	The 16 element window range block corresponding to AEU2.
Counters	Five status counters. There is actually only one set of these counters in the telemetry packet; each sweep has a copy in its table row.
FrmInd	The index within the day of the time-ordered data record containing this science frame.
Sweep	The sweep within the telemetry packet represented by this row (1 or 2).

The two AEU data blocks contain 32 elements that require more dynamic range than a single two byte integer can provide. For each of these elements, a one byte window element is provided in the AWIN blocks that essentially adds another byte of dynamic range to those measurements.

4.4 The Digital Instrument Housekeeping (DIHK) Data Table

The DIHK data table contains the DIHK packets recorded for that day. This data primarily represents digital status information relating to commands received and current status codes. Physical measurements regarding the digital electronics unit are also transmitted through this packet.

A single TOD record contains four 11.52 second DIHK telemetry packets. A row in the table represents one packet; each column represents:

Name	Description
TIME	The time of the start of the telemetry packet, represented as a modified reduced Julian day.
Data	The DIHK data portion of the packet consisting of 42 elements.
FrmInd	The index within the day of the time-ordered data record containing this science frame.
DihkInd	The index of the DIHK packet within its time-ordered data record.

4.5 The Line-Of-Sight (LOS) Table

The LOS table provides unit vectors describing the line-of-sight for each microwave horn in spacecraft coordinates. The position and attitude data [attitude provided through the quaternions] may be used with these unit vectors to determine the pointing of *WMAP* at any given time.

This table consists of a single row of twenty columns. Each column contains a three element unit vector describing the pointing of a single differencing assembly horn on either the A or B side of the spacecraft. The column names are:

K1A K1B KA1A KA1B Q1A Q1B Q2A Q2B V1A V1B
V2A V2B W1A W1B W2A W2B W3A W3B W4A W4B

4.6 Headers

Each FITS header in the file contains the conversion constant used to transform the reduced Julian day into a standard Julian day; the header keyword is TIME2JD. The primary header also contains:

- The start (keyword STIME) and end (keyword ETIME) times of the data contained by the file in a GMT text format:
YYYYDDDhhmmss
where YYYY is the year, DDD is the day of the year, hhmmss is the GMT hour, minute, and second of the day.
- The data release date (keyword RELEASE) in the same GMT format.
- The number of TOD records (keyword NUMREC) is stored in the file.

Chapter 5

Software

The *WMAP* IDL[®]¹ library is a collection of IDL[®] procedures to assist with reading, manipulating and displaying the *WMAP* data products. The library can be downloaded at:

<http://lambda.gsfc.nasa.gov>

As described in Chapter 3 all the *WMAP* maps are pixelized using the HEALPix system. The HEALPix pixelization scheme, initially developed by K. Górski, B. Wandelt, and E. Hivon, is a hierarchical equal area isolatitude pixelisation of the sphere. More information and a suite of Fortran and IDL software tools for working with HEALPix format maps is available from the HEALPix web site at:

<http://www.eso.org/science/healpix/>

5.1 FITS Readers

5.1.1 FITS_READ_MAP

The `FITS_READ_MAP` routine reads any of *WMAP* maps data product (I maps, foreground maps, etc.) into a `R*4` array. See individual data products for details.

CALLING SEQUENCE:

`FITS_READ_Map, File_Name, T, N_obs, [Header]`

INPUTS:

`File_Name` - Character name of archive map FITS file, scalar string

¹IDL[®] is a trademark of Research System, Inc., 4990 Pearl East Circle, Boulder, CO 80301: <http://www.rsinc.com>

OUTPUTS:

T - R*4 array with temperature of each pixel
 N_obs - R*4 array with number of observations of each pixel

OPTIONAL OUTPUT:

Header - FITS header with map information

EXAMPLE: Read the W4 difference assembly map

```
IDL> fits_read_map,'map_w4_imap_yr1_v1.fits',t,N_obs,h
```

5.1.2 FITS_READ_TOD

Read a WMAP time-ordered data FITS file (e.g. map_q_imap_yr1_v1.fits) into an IDL[®] structure.

CALLING SEQUENCE:

```
FITS_READ_TOD, file, arch, [/NOHK]
```

INPUTS:

file - The name of the FITS file to read.

OUTPUTS:

arch - The TOD data structure. See the function TOD_FORMAT() for additional information about this structure

OPTIONAL INPUT KEYWORD:

/NOHK - if set, then no housekeeping information is returned, and only the time stamp and science data are defined in the output structure

EXAMPLE:

Read the time-ordered data for day 221 of year 2002 into an output structure named arch

```
IDL> file ='MAP_tod_20022202357_20022212357.fits'
IDL> FITS_READ_TOD, file, arch
```

5.2 Pckt2Mnemonic()

This is a procedure to extract data for a given mnemonic from a packet in the time-ordered data (include both digital and analog housekeeping data as well as science data)

CALLING SEQUENCE:

```
data = Pckt2Mnemonic(Pckt, Mnemonic [, Status])
```

INPUTS:

Pckt - IDL structure giving Time-ordered data, e.g. as read by
FITS_READ_TOD
Mnemonic - scalar string giving the mnemonic to extract, e.g. 'DK113'

OUTPUTS:

Status - A status code: 0=success, -1=error.

RETURNED:

data - The extracted data.

OPTIONAL INPUT KEYWORDS:

/TIME - If present and nonzero, the data returned as DLBARR[N,2]
where data[* ,0] gives the WMAP reduced Julian date, and
data[* ,1] gives the extracted data. It is usually preferable
to use the TJ output keyword to obtain the Julian dates.
NFRAMES - The number of major frames over which to average detector data
or produce an rms of detector data. Only applies to science
data mnemonics beginning with 'A' (average) or 'R' (rms).
Default = 1 MF.
Other keywords are used by the various data extraction routines.

OPTIONAL OUTPUT KEYWORD:

TJ - vector of WMAP-reduced Julian dates associated with each data
point

EXAMPLE:

After reading a TOD file the Pckt2Mnemonic procedure can be used to
extract any of the mnemonics defined in Appendix B.

Extract the raw science data for channel K113 and its time base:

```
IDL> dk113_data = Pckt2Mnemonic(arch, 'dk113', tj=tj_sci)
```

Extract the major frame average for the same channel:

```
IDL> adk114_data = Pckt2Mnemonic(arch, 'adk114', tj=atj_sci)
```

Extract the temperature measured by the sensor at the top of the
A side primary (dtatoppritt):

```
IDL> trs = Pckt2Mnemonic(arch, 'dtatoppritt', tj=tj_trs)
```

5.3 Mapping Procedures

5.3.1 REPROJ_HEALPIX

This procedure converts a HealPix image to a flat map projection without doing any intensity scaling, i.e., the pixel values are in their original units.

CALLING SEQUENCE:

```
REPROJ_HEALPIX, T, Proj, Subs, [COORD=[1-9], PROJECT=[1,2],
                               SIZE=[1-5], MASK= ]
```

INPUT ARGUMENT:

T - Vector giving input HEALPix pixel list, full sky.

OUTPUT ARGUMENT:

Proj - Output reprojected map, 2-d array
 Subs - Subscripts that generate the projection from the HEALPix vector.

INPUT KEYWORDS

The following keywords are passed to GET_HEAL_LUT via _EXTRA:
 User will be prompted for the following values if they are not supplied as keywords:

COORD - Scalar Integer (1-9) giving the coordinate system transformation

	Display		
	Galactic	Celestial	Ecliptic
Native:			
Galactic	1	2	3
Celestial	4	5	6
Ecliptic	7	8	9

PROJECT - Scalar integer (1 or 2) giving the type of projection:

- 1 - Mollweide
- 2 - Zenithal Equal Area

SIZE - Scalar integer giving the size of the output image described by the table:

- 1 -- Small (512 x 256)
- 2 -- Medium (1024 x 512)
- 3 -- Large (2048 x 1024)
- 4 -- X large (4096 x 2048)
- 5 -- XX large (8192 x 4096, mollweide, native coordinates only)

OUTPUT KEYWORD:

Mask - Mask outlining the data/nondata ellipse. Same size as the output proj parameter

EXAMPLE: Display the K band all-sky map in Galactic coordinates in a

medium (1024 x 512) size Mollweide projection scaled between
-0.2 and 1.3 mK.

```
IDL> fits_read_map,'map_k_imap_yr1_v1.fits',t,n
IDL> reproj_healpix,t,proj,coord=1,project=1,size=2
IDL> tv,bytsc1(proj,-.2,1.3)
```

5.3.2 HEALINFO

This procedure prints or returns values describing HEALPix formats of varying resolution.

INPUT ARGUMENTS:

No positional arguments.

INPUT KEYWORDS:

RES: Resolution (0 - 10)
 NSIDE: Number of divisions along edge of biggest
 HEALPix pixel (1, 2, ..., 1024)
 NPIX: Total number of pixels in full sky
 (12, 48, ..., 12582912)
 SPACING: Approximate mean linear spacing between
 pixel centers in degrees
 /HELP: Flag to display short help message.

OUTPUT KEYWORDS:

These mean the same thing as the corresponding input keywords, except they are used to return results.

GET_RES
 GET_NSIDE
 GET_NPIX

5.3.3 HEALPIX_Nested_Vectors

Procedure to read Cartesian [X,Y,Z] direction vectors from (FITS) binary file for HEALPix pixel scheme, nested pixel order.

CALLING SEQUENCE:

HEALPIX_Nested_Vectors, resolution, Px, Py, Pz

INPUTS:

Resolution - Scalar integer (3-9) giving the HEALPix resolution

OUTPUTS:

Px, Py, Pz, - vectors giving the Cartesian direction vectors for the specified resolution. The number of elements will be 768, 3072, 12288, 49152, 196608, 786432 or 3145728 as the resolution is increased from 3 to 9.

5.3.4 GRID_OVERLAY

Plot coordinate grid lines on a map projection.

CALLING SEQUENCE:

```
grid_overlay, [ PROJ={'M','Z'}, IMCOORD={'G','E','C'},
              GRCOORD={'G','E','C'}, COLOR =, /PS, IMAGE=,
              LON=, LAT=, /ZBUFF ]
```

INPUTS:

none required, if defaults are satisfactory.

OUTPUTS:

output consists of a plot, either to screen or postscript file.

OPTIONAL INPUT KEYWORDS:

proj - char string - Single character specifying the projection type of the plot. Either 'M' (Mollweide) or 'Z' (Zenithal Equal Area) are allowed. Case insensitive. Defaults to 'M'.

imcoord - char string - Single character specifying the coordinate system of the image projection. Three systems are recognized: 'E' (Ecliptic J2000), 'G' (Galactic) or 'C' (Celestial J2000). Case insensitive. Defaults to 'G'.

grCOORD - char string - Single character specifying the coordinate system of the grid overlay. Three systems are recognized: 'E' (Ecliptic J2000), 'G' (Galactic) or 'C' (Celestial J2000). Case insensitive. Defaults to 'G'.

color - byte - The color (range 0-255) used to plot the grid pattern. Defaults to 0.

/ps - value=0 or 1 - Set this keyword to direct the plot to a postscript file. The output file is named 'grid_overlay.ps'. If not set, plot will be directed to the screen (windows device).

image - bytarr - A byte-scaled image over which the grid will be plotted. If not specified, the procedure will plot within the current window (screen) or plot a grid with no image to the postscript file (/ps).

lon - fltarr - lines of constant longitude, in degrees. Default is every 15 degrees centered on 0. Specifying lon=-1000. results in NO longitude lines.

```

lat - fltarr -      lines of constant latitude, in degrees.
                   Default is every 10 degrees centered on 0.
                   Specifying lat=-1000. results in NO latitude lines.

/zbuff - value=0 or 1 - Set this keyword if plotting to the z buffer
                   is desired.

```

EXAMPLE:

```

Plot ecliptic coordinates grid over the current image
IDL> grid_overlay, GRCOORD='E'

```

```

Plot a default grid (Mollweide, Galactic) over an image (Kmol1)
to a postscript file
IDL> grid_overlay,image=bytsc1(Kmol1,0,300),/ps

```

COMMENTS:

The routine scales the overlay to fill the screen window. If the user is trying to overlay an image on the screen which does not fill the window, then the overlay will be scaled incorrectly. The user need not worry about this when creating a postscript image, as the image and overlay are scaled together automatically when producing the .ps file.

The Zenithal equal area plot has a hard time plotting the lat=0 edge border. This can be remedied by plotting lat=[-0.00000001,0.000000001] in its place (and this is what the code does by default).

5.3.5 CIRCO PLOT

Plots a circle of user-requested radius over an image projection. Circle is centered on the cursor position specified either by the user clicking the left mouse button (screen) or providing a coordinate list (postscript). Option also exists to indicate *WMAP*-visible portions of circle.

CALLING SEQUENCE:

```

circoplot [,radius=radius] [,proj={'M','Z'}] [,color=num]
          [ /visible] [,coord={'G','E','C'}],
          [/ps [,image=image] [,ctable=num] [,coorlist=coorlist]

```

INPUTS:**Screen mode:**

User positions cursor over image and clicks left mouse button to specify circle center.
Routine remains active until the user clicks the right mouse button.

Postscript mode:

User provides a list of centers via coorlist keyword.

OUTPUTS:

Screen mode:

Output consists of a circle outline overlaid on an already existing image. A small cross is drawn at the requested the circle center position. Multiple circles may be drawn during the one call to circoplot. Click on right mouse button while the cursor is on the image to exit. If /visible is specified, triangles are plotted over the WMAP-visible segments of the circle.

Postscript mode:

Outputs similar to screen mode and written to file circoplot.ps. Plot symbols have been tailored for hardcopy. Postscript is written in portrait deliberately to allow user the option of using eps and preview options within ghostview.

KEYWORDS:

- radius - float - Radius of the circle, in degrees.
Default value = 141 deg.
- proj - char string - Single character specifying the projection type of the underlying image. Either 'M' (Mollweide) or 'Z' (Zenithal Equal area) are allowed. Case insensitive. Defaults to 'M'.
- color - byte - The color (range 0-255) used to plot the circle and plot symbols. Defaults to 0
- /visible - Set this keyword to have circoplot indicate those portions of the circle in which the spin axis is within 22.5 deg of the ecliptic. The result is coordinate system dependent -- see the coord keyword.
- coord - char string -THIS KEYWORD IS MEANINGFUL ONLY IF /VISIBLE IS SPECIFIED.
Single character specifying the coordinate system of the projection. Three systems are recognized: 'E' (Ecliptic J2000), 'G' (Galactic) or 'C' (Celestial J2000). Case insensitive. Defaults to 'G'.
- ps - value=0 or 1 - Set this keyword to direct the plot to a postscript file. The output file is named 'circoplot.ps'. If not set, plot will be directed to the screen (windows device).
- coorlist - fltarr - A list of circle center coordinates, in the coordinate system OF THE UNDERLYING IMAGE.

- Format is [2,N] where N is the number of centers. Must be present when /ps is requested, and is only implemented for ps at present.
- image - bytarr - A byte-scaled image over which the circles will be plotted. At present, only implemented for /ps, since user can already plot over an existing image on the screen.
- ctable - long - A number specifying which standard IDL color table to load. Only implemented for /ps.

EXAMPLE:

```
IDL> circoplot,radius=10,proj='Z',color=20
IDL> circoplot,/vis,color=100,coord='e'
IDL> circoplot,image=myimage,coorlist=[[120,50],[130,80]],/ps
```

5.3.6 PLANET_OVERLAY

Plot a cross at the position of the chosen planet over an existing image within a screen window.

CALLING SEQUENCE:

```
planet_overlay,gmt=gmt,jd=jd [,planet=planet] [,coord={'G','E','C'}]
[,proj={'M','Z'}] [,color=color]
```

INPUTS:

At minimum, use must specify a time, using either the GMT or JD keywords (but not both).

OUTPUTS:

output consists of a plot to screen.

KEYWORDS:

- gmt - char string - WMAP GMT time for which the planet position is to be computed, e.g., '200034500000'. Valid GMTs lie between 1 Nov 2000 and 20 April 2003. Do not specify GMT if you are already using the JD keyword.
- jd - scalar or vector - Julian date for which the planet position is to be computed. Only JDs between 2451849.5 and 2452749.5 are accepted. It is acceptable to input a reduced Julian date with values between 1849.4 and 2749.5. Do not specify JD if you are already using the GMT keyword.

planet - char string - Name of the planet. Only one planet may be specified. Valid planet names are 'mars', 'jupiter', 'saturn', 'uranus', 'neptune'. Default planet = 'jupiter'.

proj - char string - Single character specifying the projection type of the plot. Either 'M' (Mollweide) or 'Z' (Zenithal Equal Area) are allowed. Case insensitive. Defaults to 'M'.

coord - char string - Single character specifying the coordinate system of the projection. Three systems are recognized: 'E' (Ecliptic J2000), 'G' (Galactic) or 'C' (Celestial J2000). Case insensitive. Defaults to 'G'.

color - byte - The color (range 0-255) used to plot the scan pattern. Defaults to 0.

COMMON BLOCKS:

None.

ROUTINES CALLED:

is_ieee_big(), gmt2jul, coortrans, mollweide_xy, zea_xy

EXTERNAL FILES REFERENCED:

The FITS file JPLEPH.405 \$MAP_REF/planet_overlay/ provides the JPL DE405 ephemeris (as Chebyshev polynomials).

EXAMPLE:

To overplot Jupiter's positions for 500 days on a Galactic Mollweide projection:

```
IDL> jd0= 1850.0
IDL> planet_overlay,jd=jd0+dindgen(500)
```

COMMENTS:

The routine scales the overlay to fill the screen window. If the user is trying to overlay an image on the screen which does not fill the window, then the overlay will be scaled incorrectly.

5.4 Transformations

5.4.1 TIMETRANSFORM

Converts one time format into another.

CALLING SEQUENCE:

TimeTransform, input [, output], TransKeyword

INPUTS:

input - The input time. (See KEYWORDS for details.)

OUTPUTS:

output - The converted time. (See KEYWORDS for details.)

INPUT KEYWORDS:

- /Date2Jul - Converts a Gregorian date into reduced Julian day.
Input should be a 3-6 element array containing the date:
[year, month, day, hour, minute, second]. Time of day
elements are optional.
- /DayOfYear - Returns the day of the year for a given date. Input
should be a 3-5 element array containing the date:
[year, month, day, hour, minute]
- /DispGMT - Converts a GMT string into a more readable string.
- /DispTS - Converts a WMAP timestamp into a more human readable format

- /DOY2Date - Determines the date from day-of-year and year. Input
should be a 2 element array containing the day of year
and year. Output will be a 5 element array containing
the date: [year, month, day, hour, minute]
- /DOY2Jul - Determines the reduced Julian day from day-of-year and
year. Input should be a 2 element array containing the
day of year and year.
- /GMT2Jul - Converts a WMAP GMT date/time string into a Julian day.
- /GMT2TS - Converts a WMAP GMT into a WMAP timestamp.
- /GMT2YMD - Converts the YYYYDDD portion of a GMT string to the format
YYYY:MM:DD.
- /Jul2Date - Converts a reduced Julian day into a Gregorian date
and time. Output consists of a 6 element array containing
the date: [year, month, day, hour, minute, second].
- /Jul2GMT - Converts a reduced Julian day into a WMAP GMT date/time .
- /Jul2Tel - Converts a reduced Julian day into a telemetry structure
timestamp. The telemetry structure must already exist!
- /Tel2Jul - Converts a packet time stamp into a reduced Julian day.
- /TS2GMT - Converts a WMAP timestamp into a WMAP GMT.
- /TS2Jul - Converts an array of time stamps into reduced Julian days.

- Reference - The timestamp reference time in GMT format.
- /Verbose - If present and nonzero, the output value is written
to the screen.
- _EXTRA - IDL keyword inheritance. Keywords required by the
conversion routines can be passed directly to them
simply by specifying them in the call to this routine.

COMMENTS:

A conversion keyword indicating the type of conversion MUST be specified.

Reduced Julian days referred to here are WMAP Reduced Julian days:

Full Julian day - 2450000

EXAMPLE:

Covert the WMAP reduced Julian day extracted using Pckt2mnemonic into a GMT string YYYYDDDDhhmmsscccc000

```
IDL> adk114_data = pckt2mnemonic(arch, 'adk114', tj=atj_sci)
IDL> TimeTransform, atj_sci, GMT_string, /jul2gmt
IDL> print, GMT_string[0]
20013612359350260000
```

5.4.2 COORTRANS

Transforms between various J2000 coordinate systems. No precession is performed.

CALLING SEQUENCE:

```
coortrans,coor_in,coor_out,code [, /lonlat ]
```

INPUTS:

coor_in - fltarr OR dblarr - The input coordinates, specified either as (lon,lat) pairs or unit vector arrays. Unit vectors must be of dimension (N,3). Lonlat pairs must be of dimension (N,2).

code - char string - Character string specifying the desired coordinate transformation. Only ONE code may be requested at a time. Valid codes are:

'c2e'	- in = celestial	out = ecliptic
'e2c'	- in = ecliptic	out = celestial
'g2e'	- in = galactic	out = ecliptic
'e2g'	- in = ecliptic	out = galactic
'c2g'	- in = celestial	out = galactic
'g2c'	- in = galactic	out = celestial
'u2ll'	- in = unit vector	out = lon,lat
'll2u'	- in = lon,lat	out = unit vector

OUTPUTS:

coor_out - dblarr - The output coordinates, returned as unit vectors unless /lonlat is set by the user. Unit vectors are returned with dimension (N,3). Lonlat pairs are returned with dimension (N,2).

OPTIONAL INPUT KEYWORDS:

/lonlat - Set this keyword to get output coordinates returned as longitude,latitude pairs. (Superfluous if code = 'u2ll').

COMMON BLOCKS:

None.

ROUTINES CALLED:

get_rot_matrix()

EXAMPLE:

Transform from celestial unit vectors (x,y,z) to Galactic (lon,lat):

```
coortrans,[[x],[y],[z]],galcoor,'c2g',/lonlat
```

COMMENTS:

The routine does some rudimentary checking to ensure the input and output formats agree with the requested transformation code. It also will bounce out if the unit vectors are not normalized.

Rotation matrices are computed by the routine get_rot_matrix().

5.5 Widgets

5.5.1 MAP_DATE

This widget computes and displays dates and times in the various systems used internally by the *WMAP* project. The widget has two modes: continuous update, and calculator. The default mode is to update to the current time once per second. To enter your own data for computations, you need to stop the update, which you can do using the button **Press for Calculator Mode**.

Click on text fields to enter values in them. When you hit the **Enter** key on your keyboard, the changes will propagate through all the quantities in a reasonable way. Self-contradictory data will not mess up the computation, because the program will just use the last type of date and time that you altered. Because continuous update mode is based on system (local) time, the time zone needs to be selected with the droplist at the upper right.

5.5.2 MAPVIEW

This widget displays a HEALPix sky map, and lets the user zoom in on regions of the map on the fly.

```
IDL> mapview,file='map_w1_imap_yr1_v1.fits'
```

The widget displays two images on the right: the upper image is an all-sky map (a Mollweide projection in Galactic coordinates), with a circle drawn

over the zoomed region. The lower 512 x 512 image displays the zoomed region. The images are manipulated using the mouse cursor and the control panels on the left.

The Control panel functions are (from top to bottom)

1. **Select Map** – Choose whether to display temperature or number of observations
2. **Cursor Info** – Informational panel giving the Galactic coordinates, Healpix pixel number and pixel value of the current cursor position in either the all-sky or zoomed image. (The panel is disabled if the cursor is not over either image.)
3. **Color Scaling** - lets the user choose linear, logarithmic or histogram equalization scaling, and a color lookup table. Note temperature maps may appear entirely black with a linear scaling.
4. **Zoom Region** - User can type in the Galactic coordinates of the region to be zoomed, and then press the draw button. Alternatively, if the zoom region is selected on the all-sky map with the cursor, then the chosen coordinates are displayed. A slider allows the user to choose the area of the zoomed region; the larger the region, the smaller the zoom factor. The actual pixel scale of the zoomed region is displayed at the terminal.
5. **Quit button** - exits the widget

The mouse cursor functions are as follows: move the cursor over either the all-sky or zoomed image to have values displayed in the **Cursor Info** panel. Press any mouse button on the all sky image to define a new center for the zoomed image. Press any mouse button on the zoomed image to move that position to the center of the zoomed image.

5.6 WMAP IDL Procedures

`AIHK_Arch2Mnemonic()` Returns the physical value associated with an analog instrument housekeeping mnemonic, extracting the data from an AEU sweep from a time-ordered.

<code>AIHK_GetMnemonic()</code>	Returns a physical value associated with a mnemonic, extracting the data out of a sweep of analog instrument housekeeping telemetry data.
<code>AIHK_Pckt2Mnemonic()</code>	Return the physical value associated with an analog instrument housekeeping mnemonic, extracting the data from a DEU telemetry sweep.
<code>AIHK_Mnem2Serial</code>	Return the serial number of an analog instrument housekeeping (AIHK) PRT.
<code>AIHK_Mnem2Serial_List</code>	Returns an array of structures that associates mnemonics with serial numbers for sensor ids.
<code>AIHK_MnemTime</code>	Returns the time offset into a AIHK packet for the measurement of a given mnemonic.
<code>AIHK_MnemTimeStamp</code>	Returns an array of time stamps for a given mnemonic in an array of analog instrument housekeeping (AIHK) elements.
<code>AIHK_Mnem_Coefs</code>	Returns the conversion coefficients associated with an analog instrument housekeeping mnemonic.
<code>AIHK_Mnemonic</code>	Returns the array index of an analog instrument housekeeping mnemonic.
<code>CircOplot</code>	Overplots a circle of requested radius on a Mollweide or Zenithal equal area projection.
<code>CoorTrans</code>	Transforms input J2000 coordinates into the requested J2000 output coordinate system.
<code>CW_ImageDraw()</code>	Defines a compound widget containing a scrollable draw widget to be used to display images.
<code>CW_ImageFull()</code>	Define a compound widget containing a draw widget to be used to display entire images at reduced resolution.
<code>CW_ImageBoth()</code>	Define a compound widget to contain both a full resolution image in a scrollable draw widget and a compressed image.
<code>Date2Jul()</code>	Converts a Gregorian date and time into a reduced Julian date.
<code>DayOfYear</code>	Determines the day-of-year for a date.
<code>DefTSRef()</code>	Return the default <i>WMAP</i> timestamp reference GMT.

<code>DIHK_GetMnemonic()</code>	Returns a physical value associated with a mnemonic, extracting the data out of an array of digital instrument housekeeping telemetry data.
<code>DIHK_Pckt2Mnemonic()</code>	Returns the physical value associated with a digital instrument housekeeping mnemonic, extracting the data from a DEU telemetry packet.
<code>DIHK_Mnemonic()</code>	Returns the array index of a digital instrument housekeeping mnemonic.
<code>DIHK_Mnem_Coefs</code>	Returns the conversion coefficients associated with a digital instrument housekeeping (DIHK) mnemonic. Automatically written.
<code>DispGMT()</code>	Converts a time formatted as a <i>WMAP</i> GMT into a more human-readable form.
<code>DispTS()</code>	Converts a <i>WMAP</i> timestamp into a more human readable format.
<code>DOY2Date</code>	Converts a year and day-of-year into a five element date vector. This is the reverse of <code>dayofyear.pro</code> .
<code>DOY2Jul</code>	Converts a year and day-of-year into a <i>WMAP</i> Reduced Julian day.
<code>extract_band_index</code>	Extracts the frequency band and array index value from an input channel string. Supporting routine for <code>sci_getmnemonic</code> .
<code>frame_avg()</code>	Computes single or multiple frame averages of science data. Supporting routine for <code>sci_getmnemonic</code> .
<code>frame_rms()</code>	Computes single or multiple frame rms of science data. Supporting routine for <code>sci_getmnemonic</code> .
<code>FITS_Read_TOD</code>	Read time ordered archive data from a binary FITS table.
<code>FITS_Read_Map</code>	IDL procedure to read <i>WMAP</i> archive-format sky maps.
<code>Get_DEU_Int_Temp</code>	Converts DEU internal temperature from counts to degrees Centigrade via a lookup table.
<code>Get_Heal_LUT</code>	Procedure to read and return a user-selectable look-up table.

Get_Heal_RES()	Function to compute the resolution of a healpixelized sky map, given the number of map pixels.
Get_PRT_Temp	Converts PRT resistance in ohms to temperature in Kelvin, given the PRT serial number.
Get_Rot_Matrix()	Returns rotation matrix for conversion between the specified input and output coordinate systems.
GMT2Jul()	Converts a WMAP GMT datetime string into a reduced Julian date.
GMT2TS	Converts a WMAP GMT into a WMAP timestamp.
GMT2YMD	Converts the YYYYDDD portion of a WMAP GMT string into a string of format YYYYM-MDD.
Grid_Overlay	Overplots coordinate grid on a Mollweide or Stereographic projection.
HEALinfo	IDL procedure to return or print information on HEALPix resolutions.
HEALPIX_Nested_Vectors	IDL procedure to read Cartesian [X,Y,Z] direction vectors from binary file for HEALPix pixel scheme, nested pixel order.
Jul2Date	Converts a reduced Julian date into a Gregorian date and time. Unlike a classic reduced Julian date, the full Julian date is recovered by adding 2450000.
HealPix_to_Image	Convert a 1-d Healpix map into a 2-d byte-scaled image ready for display.
Jul2GMT()	Converts a WMAP GMT date/time string into a Julian date.
Jul2Tel	Converts a WMAP Reduced Julian day into a telemetry structure timestamp.
Jul2TS()	Converts a WMAP Reduced Julian day into a time stamp.
KeyArray()	Breaks a string containing a number of comma-delimited elements into an array of strings.
KeyFile	Reads a file containing keywordvalue pairs into an array of structures, each element of which contains a keywordvalue pair.

KeyParse	Breaks a string into a keywordvalue pair.
LoadCT_012	Load a standard IDL color table with the first three colors reserved as white, black and gray.
Load_MAP_Params	Reads the contents of the general WMAP program parameters file into an IDL structure.
MAP_Date	Widget to convert the various WMAP time and date formats.
MAPView	Interactive widget to display and zoom a HealPix map.
Mnem_Type()	Function to return the type of mnemonic associated with an input mnemonic, eg. AIHK, SCI, etc..
mollweide()	Computes Mollweide angle theta from input latitudes.
mollweide_xy	Converts longitude and latitude coordinates to x,y positions on a Mollweide projection.
Now2Jul()	Returns the current system time as a WMAP Reduced Julian day.
Pckt2Mnemonic()	Returns the physical value associated with a WMAP telemetry mnemonic. This is a wrapper routine that calls the appropriate specific routine depending on mnemonic type.
Planet_Overlay	Plots a planet's position on an existing skymap within a screen window.
projxy2coord	Converts (x,y) positions on a Mollweide or Zenithal Equal Area projection to longitude and latitude.
rotx()	Computes rotation matrix for rotation about x axis.
rotz()	Computes rotation matrix for rotation about z axis.
Sci_GetMnemonic()	Extracts a channel of radiometer data from an array of science packets. Depending on mnemonic prefix,the routine can also return a frame average or rms.
Sci_Mnemonic()	Tests whether or not a given science mnemonic is valid.

ScrTV	Displays an image in a scrollable draw widget. This allows the user to examine a full resolution portion of the image, using the scrollbars to navigate around.
Tel2Jul()	Converts a <i>WMAP</i> telemetry structure time stamp into a reduced Julian date.
TimeTransform	Converts one time format into another.
TS2GMT	Converts a <i>WMAP</i> timestamp into a <i>WMAP</i> GMT.
TS2Jul()	Converts a time stamp into a <i>WMAP</i> Reduced Julian day.
Reproj_HealPix	Convert a HealPix image to a flat map projection.
spread_pkt_tjul()	Propagate science packet times in reduced Julian format to each observation within a packet. Supporting routine for sci_getmnemonic.
TextRead	TextRead reads a non-empty recordline from an open text file. Lines are read until a nonzero length string is read.
TimeStamp_AddTime	Adds to a <i>WMAP</i> Omega time stamp.
timestamp_diff()	Determine the difference between two time stamps.
tod_format()	Defines the time-ordered data (TOD) structure format.
Xcolors	Interactively change color tables (from David Fanning's Library).
zea_xy	Converts longitude and latitude coordinates to x,y positions on a Zenithal equal area projection.

Routines to give the *WMAP* pointing direction at a given time (using the quaternions in the time-ordered data) are expected to be available in the next software release.

Bibliography

- ADAMO, R. C. AND MATARRESE, J. R., 1983. “Transient Pulse Monitor Data from the P78-2 (SCATHA) Spacecraft”. *J Spacecraft* **20(5)**:432.
- BARNES, C., LIMON, M., PAGE, L., BENNETT, C., BRADLEY, S., HALPERN, M., HINSHAW, G., JAROSIK, N., JONES, W., KOGUT, A., MEYER, S., MOTRUNICH, O., TUCKER, G., WILKINSON, D., AND WOLLACK, E., 2002. “The MAP Satellite Feed Horns”. *ApJS* **143**:567.
- BARNES, C. ET AL., 2003. “First Year Wilkinson Microwave Anisotropy Probe (WMAP) Observations: Characterization of the Far-Sidelobes”. *ApJ* Submitted.
- BENNETT, C. L., BAY, M., HALPERN, M., HINSHAW, G., JACKSON, C., JAROSIK, N., KOGUT, A., LIMON, M., MEYER, S. S., PAGE, L., SPERGEL, D. N., TUCKER, G. S., WILKINSON, D. T., WOLLACK, E., AND WRIGHT, E. L., 2003a. “The *Microwave Anisotropy Probe* Mission”. *ApJ* **583**:1.
- BENNETT, C. L., HALPERN, M., HINSHAW, G., JAROSIK, N., KOGUT, A., LIMON, M., MEYER, S. S., PAGE, L., SPERGEL, D. N., TUCKER, G. S., WOLLACK, E., WRIGHT, E. L., BARNES, C., GREASON, M., HILL, R., KOMATSU, E., NOLTA, M., ODEGARD, N., PEIRIS, H., VERDE, L., AND WEILAND, J., 2003b. “First Year Wilkinson Microwave Anisotropy Probe (WMAP) Observations: Maps and Basic Results”. *ApJ* Submitted.
- BENNETT, C. L. ET AL., 2003c. “First Year Wilkinson Microwave Anisotropy Probe (WMAP) Observations: Foreground Emission”. *ApJ* Submitted.
- FREDERICKSON, A. R., 1996a. “Correction to Upsets Related to Spacecraft Charging”. *IEEE Transactions on Nuclear Science* **43(4)**:2454.

- FREDERICKSON, A. R., 1996b. "Upsets Related to Spacecraft Charging". *IEEE Transactions on Nuclear Science* **43(2)**:426.
- GILMORE, D. G. AND BELLO, M., 1994. *Satellite Thermal Control Handbook*, chap. 4. The Aerospace Corporation Press, El Segundo, CA.
- HINSHAW, G. F. ET AL., 2003a. "First Year Wilkinson Microwave Anisotropy Probe (WMAP) Observations: Data Processing and Systematic Error Limits". *ApJ* Submitted.
- HINSHAW, G. F. ET AL., 2003b. "First Year Wilkinson Microwave Anisotropy Probe (WMAP) Observations: The Angular Power Spectrum". *ApJ* Submitted.
- JACKSON, C., 2002. "Microwave Anisotropy Probe (MAP) Observatory Launch & In-Orbit Checkout (L&IOC) Phase, Volume I: Summary Report". Tech. rep., NASA/GSFC.
- JAROSIK, N. ET AL., 2003a. "Design, Implementation and Testing of the MAP Radiometers". *ApJS* **145**.
- JAROSIK, N. ET AL., 2003b. "First Year Wilkinson Microwave Anisotropy Probe (WMAP) Observations: In-Orbit Radiometer Characterization". *ApJ* Submitted.
- JIMENEZ, R. D., 1988. "Natural Environment Charged Particle Heating of Spacecraft Cryogenic Components". Tech. Rep. TOR-0088(3062)-3, The Aerospace Corporation.
- KOGUT, A. ET AL., 2003. "First Year Wilkinson Microwave Anisotropy Probe (WMAP) Observations: TE Polarization". *ApJ* Submitted.
- KOMATSU, E. ET AL., 2003. "First Year Wilkinson Microwave Anisotropy Probe (WMAP) Observations: Test of Gaussianity". *ApJ* Submitted.
- KOONS, H. C. AND CHIN, T. S., 1994. "Broadband Radio-Frequency Spectrum from Electrostatic Discharges on Spacecraft". *J Spacecraft* **31(3)**:528.
- LEUNG, P. AND PLAMP, G., 1982. "Characteristics of RF Resulting from Dielectric Discharges". *IEEE Transactions on Nuclear Science* **29(6)**:1610.
- LEUNG, P. ET AL., 1986. "Environment-Induced Electrostatic Discharges as the Cause of Voyager 1 Power-On Resets". *J Spacecraft* **23(3)**:323.

- MIZERA, P. F., 1983. "A Summary of Spacecraft Charging Results". *J Spacecraft* **20(5)**:438.
- PAGE, L. ET AL., 2003a. "First Year Wilkinson Microwave Anisotropy Probe (WMAP) Observations: Beam Profiles and Window Functions". *ApJ* Submitted.
- PAGE, L. ET AL., 2003b. "First Year Wilkinson Microwave Anisotropy Probe (WMAP) Observations: Interpretation of the TT and TE Angular Spectrum Peaks". *ApJ* Submitted.
- PAGE, L. ET AL., 2003c. "The Optical Design and Characterization of the Microwave Anisotropy Probe". *ApJ* **585**:in press.
- PEIRIS, H. ET AL., 2003. "First Year Wilkinson Microwave Anisotropy Probe (WMAP) Observations: Implications for Inflation". *ApJ* Submitted.
- SPERGEL, D. N. ET AL., 2003. "First Year Wilkinson Microwave Anisotropy Probe (WMAP) Observations: Cosmological Parameters from CMB and Large Scale Structure". *ApJ* Submitted.
- STARIN, S. R., O'DONNELL, JR., J. R., WARD, D. K., WOLLACK, E. J., BAY, P. M., AND FINK, D. R., 2002. "An Anomalous Force on the MAP Spacecraft". In *AIAA Symposium*. Monterey, CA.
- TRIOLO, J. J., HEANEY, J. B., AND HASS, G., 1977. "Coatings in Space Environment". *SPIE Optics in Adverse Environments* **121**:46.
- VAMPOLA, A. L., JIMENEZ, R. D., AND COX, J. E., 1989. "Heat Loads Due to Space Particle Environment". *Spacecraft* **26(6)**:474.
- VERDE, L. ET AL., 2003. "First Year Wilkinson Microwave Anisotropy Probe (WMAP) Observations: Parameter Estimation Methodology". *ApJ* Submitted.
- WRIGHT, E., 1996. "Scanning and Mapping Strategies for CMB Experiments" astro-ph/9612006.
- WRIGHT, E. L., HINSHAW, G., AND BENNETT, C. L., 1996. "Producing Megapixel Cosmic Microwave Background from Differential Radiometer Data". *ApJ* **458**:L53.

Appendix A

Selected *WMAP* Log Entries

This appendix consists of selected entries from the events log that the members of the Science Working Group have kept throughout the mission. This particular subset of the log lists all major events from the beginning of the Pre-ship Functional Test (April 6, 2001) to the end of the one year in-flight operations.

Selected MAP Satellite Pre-Flight Preparations:

...

GMT 20010961125	GSFC: Pre-Ship Functional Test (GSFC)
GMT 20011161100	SAEF-2: Post-Ship Functional and CPT (KSC)
GMT 20011621058	SAEF-2: Instrument Contingency Tests (KSC)
GMT 20011721430	SLC17B: Pre-Fairing Pad Functional Test (KSC)
GMT 20011780851	SLC17B: Post-fairing Pad Functional Test (KSC)
GMT 20011791200	SLC17B: Load Vehicle Oxidizer
GMT 20011811013	SLC17B: Instrument Pre-Flight Burn-in
GMT 20011811803	SLC17B: Load Vehicle LOX
GMT 20011811925	SLC17B: Poll to go to Launch Decision Authority (KSC/GSFC)
GMT 20011811929	SLC17B: GSFC poll to Proceed with Terminal Count (GSFC)
GMT 20011811939	SLC17B: Proceed to internal power (KSC/GSFC)

Selected MAP Satellite Launch and In-Orbit Checkout (IOC):

GMT 20011811946	MAP Launch Time: 2001181194646.183
GMT 20011811951	Main engine cutoff/fairing separation...
GMT 20011812000	SECO-I cutoff -- trajectory is on course...
GMT 20011812100	MAP Transmitter detected by TDRS...
GMT 20011812103	Solar arrays deployed...
GMT 20011812138	Star trackers powered...
GMT 20011812143	MAP Instrument powered...

GMT 20011821515 Gyro calibration slews...
GMT 20011830744 MAP Thruster Tests...
GMT 20011831918 Enter observing mode for the first time:
CMB Dipole/galaxy visible in science data
Begin mapping sidelobes with Moon as source
GMT 20011842201 Top Radiator PRT (DTAMXTOPRADT) fails open.
GMT 20011890153 P1 - First Perigee Maneuver
GMT 20011890244 End mapping sidelobes with Moon as source
GMT 20011980143 P2 - Second Perigee Maneuver
GMT 20012021758 A3 - Second Apogee Maneuver (third apogee)
GMT 20012070832 PF - Final Perigee Maneuver
GMT 20012080330 PF'- Final Perigee Correction
GMT 20012080200 PF"- Final Perigee Correction
GMT 20012111639 Lunar Swing-by
GMT 20012181551 Mid-Course Correction #1
GMT 20012181819 W411 Bias Adjustment.
GMT 20012191300 Turn off the omni antenna and switch to the
medium gain antenna. FPA is observed to accelerate
its cooling. Leave transmitter power to allow ranging.
GMT 20012191807 W411 Returned to Nominal Bias Setting.
GMT 20012210306 W12 Science Output Jump: Sudden jump of W12 science
output, both channels W123 and W124 jumped of about
35-40 counts in opposite directions. When calibrated
the jump is about 100mK. The jump is essentially
instantaneous, it happens across just one sample and
the dipole is visible before and after the jump. No
changes in drain currents or RF bias are present at the
time of the output jump. No change noted in other science
channels. Observed radiometric signature is consistent
with relief of thermally induced stress in radiometer and
is anticipated in this phase of mission operations. This
and any other subsequent suspect data to be flagged in
time stream data mask.

START: MAP YEAR-ONE SCIENCE DATA

Transmitter Make-Up Heater Tests

GMT 20012212000 Turn off transmitter: Today we turn off the transmitter
for the first time in flight and will turn on the
transponder make-up heater when the transmitter is off.
GMT 20012410810 After flying with the transmitter make-up heater for
several days, we conclude that the daily thermal cycling
seen in the instrument boxes is probably worse than the
potential "RFI", and wear on tear on the transmitter. The
transmitter will now remain on for the duration of the

mission, effective with this pass. Continue the cruise to L2 in this configuration.

Mid-Course Correction #2

GMT 20012571620 Start Mid-course correction #2: This is a very small maneuver of about 4.3 cm/sec Delta V. Thrusters #1&2 will be fired for about 6.44sec.
The burn will occur at 16:37 GMT.
Exit observing mode. Command to spin down at the desired precession angle. Sun angle remains at 22.5 degrees for now. The S/C will shortly be commanded to the desired spin angle.

GMT 20012571625 Command S/C to inertial - this sets up the command to the correct spin angle and will result in a short excursion from 22.5 degrees during the slew.

GMT 20012571627 Actual slew to the correct spin angle.

GMT 20012571635 Slew to 19 degrees in preparation for the burn.

GMT 20012571637 Burn starts and stops. 6.4 seconds.

GMT 20012571639 Return to inertial hold.

GMT 20012571640 Disable thrusters. Enable ACS rate checks.

GMT 20012571641 Slewing back to 22.5 degrees.

GMT 20012571644 Disable thrusters. Restart TSMs.

GMT 20012571701 Send command to resume observing mode.

End Mid-Course Correction #2

Solar Proton Storm

GMT 20012671200 A severe solar storm has occurred with >10 MeV proton fluxes reaching 10^5 times normal levels. We are observing a heating of the cold stage of several tens of millikelvins with a heating slope that appears to be well correlated with the proton flux. Since this thermal perturbation is larger than the mid-course correction #2 we may want to cut a period of data about this time. The storm itself will likely last for a few days.

ASTB Thermal Change

GMT 200128900 Star tracker crosses internal thermal threshold of CCD thermo-electric cooler. ASTB baseplate cools 4C from 30C to 26C. Change in thermal distribution causes RXB to cool by ~10mK.

Solar Proton Storm

GMT 20013100258 The second severe solar storm since MAP's launch has occurred with >10 MeV proton fluxes reaching >10⁵ times normal levels. This is more severe than the previous storm on 2001267. This storm caused an apparent single event upset (possibly on the power-up reset circuit in the MAC) which caused a power-up cold restart of the Mongoose. All recorded data was lost from the start of the previous pass to the time of the reset.
Telemetry Lost: 20013100258 - 20013101635.

GMT 20013101430 The entry into safhold was noticed on the subsequent pass which started at 20011430. After spending some time diagnosing the problem, we are preparing to exit safhold and reenter observing mode ~20013101830. The telemetry from the time of the reset until the clock was re-jammed at 20013101542 has a time stamp in 1994.

GMT 20013101742 Command out of safhold to sun-acquisition mode.

GMT 20013101823 Command back to inertial mode.

GMT 20013101825 Slew to 22.5 degrees off the Sun line.

GMT 20013101834 Command to observing mode.

GMT 20013101838 Achieved observing mode.

GMT 20013101903 Adjust clock 1Hz deviation.

GMT 20013101913 Complete clock adjustment.

GMT 20013101943 Return to normal operations.

Solar Proton Storm

GMT 200132800 A severe solar storm has occurred with >10 MeV proton fluxes reaching 10⁵ times normal levels. We are observing a heating of the cold stage of several tens of millikelvins with a heating slope that appears to be well correlated with the proton flux. Since this thermal perturbation is larger than the mid-course correction #2 we may want to cut a period of data about this time. The storm itself will likely last for a few days.

Station-Keeping Maneuver #1 (SK1)

GMT 20020161620 This is a small maneuver of 42.8 cm/sec delta V that will last for 72 sec.
Thrusters #3&4 will be fired at 16:50 GMT.
Turn on catbed heaters in preparation for the burn.

GMT 20020161624 Brief drop-out of telemetry.

GMT 20020161633 Exit observing mode. Command to spin down at the desired precession angle. Sun angle remains at 22.5 degrees for

now. The S/C will shortly be commanded to the desired spin angle.

GMT 20020161638 Command to go inertial - this sets up the command to the correct spin angle and will result in a small excursion from 22.5 degrees during the slew.

GMT 20020161639 Actual slew to the correct spin angle.

GMT 20020161648 Slew to 19 degrees in preparation for the burn.

GMT 2002016165055 Burn starts, lasts 72 seconds, as planned.

GMT 20020161652 Return to inertial hold.

GMT 20020161653 Disable thrusters. Enable ACS rate checks.

GMT 20020161656 Return to observing mode 5 minutes after burn.

End Station-Keeping Maneuver #1 (SK1)

Reaction Wheel 3 Temperature Increase

GMT 2002054 Reaction Wheel 3 bearing temperature increased by about 1.2K and the corresponding wheel's flange by about ~1K. ACS attributes this behavior to movement of the bearings' lubricant. Previous flight experience with this design suggests that this behavior is anticipated.

Battery Anomaly

GMT 2002054 Around this day the battery differential voltage started to deviate from its nominal value. Evidence suggests that effect is due to a partially shorted cell.

GMT 2002058 The S/C responds to the continuous raise of the differential voltage by resetting the battery VT curve to VT0 per design.

Reaction Wheel 1 Temperature Increase

GMT 2002075 At ~20020750445 the drag torque level and the temperatures of both bearing and flange of RWA stepped up by about 0.002 Nm 1 C respectively. Have seen similar changes in the past and they are not considered an anomaly.

Station-Keeping Maneuver #2 (SK2)

GMT 20021281533 This is a small maneuver of 34.8 cm/sec delta V that will last for 49 sec.
Thrusters #1&2 will be fired at 16:03 GMT.

Turn on catbed heaters in preparation for the burn.

GMT 20021281546 Exit observing mode. Command to spin down at the desired precession angle. Sun angle remains at 22.5 degrees for now. The S/C will shortly be commanded to the desired spin angle.

GMT 20021281551 Command to go inertial -- this sets up the command to the correct spin angle and will result in a small excursion from 22.5 degrees during the slew.

GMT 20021281552 Actual slew to the correct spin angle.

GMT 20021281601 Slew to 19 degrees in preparation for the burn.

GMT 2002128160327 Burn starts, lasts 49 seconds, as planned.

GMT 20021281604 Return to inertial hold.

GMT 20021281609 Disable thrusters. Enable ACS rate checks.

GMT 20021281610 Slew back to 22.5 degrees in preparation for observing mode.

GMT 20021281612 Return to observing mode 5 minutes after burn.

End Station-Keeping Maneuver #2 (SK2)

GMT 20021582120 Shift in nominal AEU/DEU temperature of ~28mK observed in PRTs sensors. Source localized near DVA223_4AMPT PRT sensor from spatial and temporal evolution of observed event. Estimate change in card power dissipation of ~+0.1%. Correlated response in science data is not detected.

Station-Keeping Maneuver #3 (SK3)

GMT 20022111608 This is a small maneuver of 45.98 cm/sec delta V that will last for 66 sec.
Thrusters #1&2 will be fired at 16:38:45 GMT.
Turn on catbed heaters in preparation for the burn.

GMT 20022111621 Exit observing mode. Command to spin down at the desired precession angle. Sun angle remains at 22.5 degrees for now. The S/C will shortly be commanded to the desired spin angle.

GMT 20022111626 Command to go inertial - this sets up the command to the correct spin angle and will result in a small excursion from 22.5 degrees during the slew.

GMT 20022111627 Actual slew to the correct spin angle.

GMT 20022111635 Disable RTS 181, system rate checks.

GMT 20022111636 Slew to 19 degrees in preparation for the burn.

GMT 2002211163845 Burn starts, lasts 66 seconds, as planned.

GMT 20022111640 Return to inertial hold.

GMT 20022111642 Disable thrusters. Enable ACS rate checks.

GMT 20022111642 Disable catbed heaters.

GMT 2002211164245 Slew back to 22.5 degrees in preparation for observing mode.

GMT 20022111646 Return to observing mode 4 minutes after burn, 26 minutes
 after leaving observing mode.

 End Station-Keeping Maneuver #3 (SK3)

GMT 2002222 End of year-one data

END: MAP YEAR-ONE DATA

Appendix B

Mnemonics Lists

Signals in the *WMAP* telemetry are uniquely identified by a set of mnemonics. Identifying a specific signal using its mnemonic allows the user to extract it from a more complex data structure using software routines which are provided (see Chapter 5). The main signals of interest in the *WMAP* time-ordered data are described by the science and the housekeeping mnemonics, these are all listed in this appendix grouped by their functionalities. For the mnemonics associated with a temperature sensor the description field indicates the approximate position of that sensor on the observatory.

B.1 Science Mnemonics

Raw Data	Major Frame First Point	Major Frame Average	Major Frame RMS
DK113	QDK113	ADK113	RDK113
DK114	QDK114	ADK114	RDK114
DK123	QDK123	ADK123	RDK123
DK124	QDK124	ADK124	RDK124
DKA113	QDKA113	ADKA113	RDKR113
DKA114	QDKA114	ADKA114	RDKR114
DKA123	QDKA123	ADKA123	RDKR123
DKA124	QDKA124	ADKA124	RDKR124
DQ113	QDQ113	ADQ113	RDQ113
DQ114	QDQ114	ADQ114	RDQ114
DQ123	QDQ123	ADQ123	RDQ123
DQ124	QDQ124	ADQ124	RDQ124
DQ213	QDQ213	ADQ213	RDQ213
DQ214	QDQ214	ADQ214	RDQ214
DQ223	QDQ223	ADQ223	RDQ223
DQ224	QDQ224	ADQ224	RDQ224
DV113	QDV113	ADV113	RDV113
DV114	QDV114	ADV114	RDV114
DV123	QDV123	ADV123	RDV123
DV124	QDV124	ADV124	RDV124
DV213	QDV213	ADV213	RDV213
DV214	QDV214	ADV214	RDV214
DV223	QDV223	ADV223	RDV223
DV224	QDV224	ADV224	RDV224
DW113	QDW113	ADW113	RDW113
DW114	QDW114	ADW114	RDW114
DW123	QDW123	ADW123	RDW123
DW124	QDW124	ADW124	RDW124
DW213	QDW213	ADW213	RDW213
DW214	QDW214	ADW214	RDW214
DW223	QDW223	ADW223	RDW223
DW224	QDW224	ADW224	RDW224
DW313	QDW313	ADW313	RDW313
DW314	QDW314	ADW314	RDW314
DW323	QDW323	ADW323	RDW323
DW324	QDW324	ADW324	RDW324
DW413	QDW413	ADW413	RDW413
DW414	QDW414	ADW414	RDW414
DW423	QDW423	ADW423	RDW423
DW424	QDW424	ADW424	RDW424

B.2 Instrument Housekeeping Mnemonics

B.2.1 Amplifier Drain Currents

Mnemonic	Description	Mnemonic	Description
DFK111B8DNI	K111 FPA	DFV211B9DNI	V211 FPA
DFK112B8DNI	K112 FPA	DFV212B9DNI	V212 FPA
DFK121B8DNI	K121 FPA	DFV221B9DNI	V221 FPA
DFK122B8DNI	K122 FPA	DFV222B9DNI	V222 FPA
DRK111B8DNI	K111 RXB	DRV211B9DNI	V211 RXB
DRK112B8DNI	K112 RXB	DRV212B9DNI	V212 RXB
DRK121B8DNI	K121 RXB	DRV221B9DNI	V221 RXB
DRK122B8DNI	K122 RXB	DRV222B9DNI	V222 RXB
DFKA111B3DNI	Ka111 FPA	DFW111B4DNI	W111 FPA
DFKA112B3DNI	Ka112 FPA	DFW112B4DNI	W112 FPA
DFKA121B3DNI	Ka121 FPA	DFW121B4DNI	W121 FPA
DFKA122B3DNI	Ka122 FPA	DFW122B4DNI	W122 FPA
DRKA111B3DNI	Ka111 RXB	DRW111B4DNI	W111 RXB
DRKA112B3DNI	Ka112 RXB	DRW112B4DNI	W112 RXB
DRKA121B3DNI	Ka121 RXB	DRW121B4DNI	W121 RXB
DRKA122B3DNI	Ka122 RXB	DRW122B4DNI	W122 RXB
DFQ111B1DNI	Q111 FPA	DFW211B5DNI	W211 FPA
DFQ112B1DNI	Q112 FPA	DFW212B5DNI	W212 FPA
DFQ121B1DNI	Q121 FPA	DFW221B5DNI	W221 FPA
DFQ122B1DNI	Q122 FPA	DFW222B5DNI	W222 FPA
DRQ111B1DNI	Q111 RXB	DRW211B5DNI	W211 RXB
DRQ112B1DNI	Q112 RXB	DRW212B5DNI	W212 RXB
DRQ121B1DNI	Q121 RXB	DRW221B5DNI	W221 RXB
DRQ122B1DNI	Q122 RXB	DRW222B5DNI	W222 RXB
DFQ211B10DNI	Q211 FPA	DFW311B6DNI	W311 FPA
DFQ212B10DNI	Q212 FPA	DFW312B6DNI	W312 FPA
DFQ221B10DNI	Q221 FPA	DFW321B6DNI	W321 FPA
DFQ222B10DNI	Q222 FPA	DFW322B6DNI	W322 FPA
DRQ211B10DNI	Q211 RXB	DRW311B6DNI	W311 RXB
DRQ212B10DNI	Q212 RXB	DRW312B6DNI	W312 RXB
DRQ221B10DNI	Q221 RXB	DRW321B6DNI	W321 RXB
DRQ222B10DNI	Q222 RXB	DRW322B6DNI	W322 RXB
DFV111B2DNI	V111 FPA	DFW411B7DNI	W411 FPA
DFV112B2DNI	V112 FPA	DFW412B7DNI	W412 FPA
DFV121B2DNI	V121 FPA	DFW421B7DNI	W421 FPA
DFV122B2DNI	V122 FPA	DFW422B7DNI	W422 FPA
DRV111B2DNI	V111 RXB	DRW411B7DNI	W411 RXB
DRV112B2DNI	V112 RXB	DRW412B7DNI	W412 RXB
DRV121B2DNI	V121 RXB	DRW421B7DNI	W421 RXB
DRV122B2DNI	V122 RXB	DRW422B7DNI	W422 RXB

B.2.2 Radiometer RF Bias (Total Power)

Mnemonic	Description
DRK113RFBI0	K113 RF bias
DRK114RFBI1	K114 RF bias
DRK123RFBI2	K123 RF bias
DRK124RFBI3	K124 RF bias
DRKA113RFBI36	Ka113 RF bias
DRKA114RFBI37	Ka114 RF bias
DRKA123RFBI38	Ka123 RF bias
DRKA124RFBI39	Ka124 RF bias
DRQ113RFBI20	Q113 RF bias
DRQ114RFBI21	Q114 RF bias
DRQ123RFBI22	Q123 RF bias
DRQ124RFBI23	Q124 RF bias
DRQ213RFBI28	Q213 RF bias
DRQ214RFBI29	Q214 RF bias
DRQ223RFBI30	Q223 RF bias
DRQ224RFBI31	Q224 RF bias
DRV113RFBI32	V113 RF bias
DRV114RFBI33	V114 RF bias
DRV123RFBI34	V123 RF bias
DRV124RFBI35	V124 RF bias
DRV213RFBI12	V213 RF bias
DRV214RFBI13	V214 RF bias
DRV223RFBI14	V223 RF bias
DRV224RFBI15	V224 RF bias
DRW113RFBI4	W113 RF bias
DRW114RFBI5	W114 RF bias
DRW123RFBI2	W123 RF bias
DRW124RFBI3	W124 RF bias
DRW213RFBI24	W213 RF bias
DRW214RFBI25	W214 RF bias
DRW223RFBI26	W223 RF bias
DRW224RFBI27	W224 RF bias
DRW313RFBI16	W313 RF bias
DRW314RFBI17	W314 RF bias
DRW323RFBI18	W323 RF bias
DRW324RFBI19	W324 RF bias
DRW413RFBI8	W413 RF bias
DRW414RFBI9	W414 RF bias
DRW423RFBI10	W423 RF bias
DRW424RFBI11	W424 RF bias

B.2.3 TRS Temperatures

Mnemonic	Description
DTATOPPRIT	A side primary temp (top)
DTAMIDPRIT	A side primary temp (middle)
DTATOPSECT	A side secondary temp (top)
DTAMIDSECT	A side secondary temp (middle)
DTABOTSECT	A side secondary temp (bottom)
DTBTOPPRIT	B side primary temp (top)
DTBMIDPRIT	B side primary temp (middle)
DTBTOPSECT	B side secondary temp (top)
DTBMIDSECT	B side secondary temp (middle)
DTAPXMIDRADT	+X radiator, A side temp (middle)
DTBPMIDRADT	+X radiator, B side temp (middle)
DTAMXTOPRADT	-X radiator, A side temp (top)
DTBMXBOTRADT	-X radiator, B side temp (bottom)

B.2.4 FPA Temperatures

Mnemonic	Description
DFK1AFEEDT	K1 A side feed temp (upper)
DFW3BFEEDT	W3 B side feed temp (middle)
DFQ1AFEEDT	Q1 A side feed temp (lower)
DFKA1BFEEDT	Ka1 B side feed temp (upper)
DFW3AFEEDT	W3 A side feed temp (middle)
DFQ2BFEEDT	Q2 B side feed temp (lower)
DFK1BOMTT	K1 B side OMT temp (upper)
DFW3AOMTT	W3 A side OMT temp (middle)
DFQ1BOMTT	Q1 B side OMT temp (lower)
DFKA1AOMTT	Ka1 A side OMT temp (upper)
DFW3BOMTT	W3 B side OMT temp (middle)
DFQ2AOMTT	Q2 A side OMT temp (lower)
DFV11FPATEET	V11 FPA magic tee temp
DFV22FPATEET	V22 FPA magic tee temp
DFW11FPATEET	W11 FPA magic tee temp
DFW22FPATEET	W22 FPA magic tee temp
DFW32FPATEET	W32 FPA magic tee temp

B.2.5 RXB Temperatures

Mnemonic	Description
DRV111RXBAMPT	V111 RXB amplifier temp
DRV222RXBAMPT	V222 RXB amplifier temp
DRW111RXBAMPT	W111 RXB amplifier temp
DRW221RXBAMPT	W221 RXB amplifier temp
DRW321RXBAMPT	W321 RXB amplifier temp
DRK12RXBRIBT	K12 RXB rib temp
DRKA12RXBRIBT	Ka12 RXB rib temp
DRQ1RXBRIBT	Q1 RXB rib temp
DRQ2RXBRIBT	Q2 RXB rib temp
DRW3RXBRIBT	W3 RXB rib temp
DRPYPSHPRTKT	+Y phase switch driver board temp
DRMYPSPRRTKT	-Y phase switch driver board temp

B.2.6 AEU Temperatures

Mnemonic	Description
DAW323_4AMPT	W3 board temp between 23/24 amps
DAW2_14_23AMP_ADT	W2 board temp between 14/23 amps & a/d
DAV113_4ADT	V1 board temp between 13/14 a/d's
WDAW113_4ADT	W1 board temp between 13/14 a/d's
DAV223_4AMPT	V2 board temp between 23/24 amps
DAQ113_4ADT	Q1 board temp between 13/14 a/d's
DAIHK1BDT	Housekeeping board 1 temp
DAIHK2BDT	Housekeeping board 2 temp
DACONVBDT	Power converter board temp

B.2.7 PDU Temperatures

Mnemonic	Description
DPPINTT1	PDU internal temperature #1
DPPINTT2	PDU internal temperature #2
DPPINTT3	PDU internal temperature #3
DPV111_2FPAT	V111/2 FPA regulator board temp
DPW221_2FPAT	W221/2 FPA regulator board temp
DPW321_2FPAT	W321/2 FPA regulator board temp
DPV221_2RXBT	V221/2 RXB regulator board temp
DPW111_2RXBT	W111/2 RXB regulator board temp
DPW321_2RXBT	W321/2 RXB regulator board temp

B.2.8 AEU Voltages and Reference Roads

Mnemonic	Description
DAP15VBD1	Housekeeping board 1 +15V converter
DAM15VBD1	Housekeeping board 1 -15V converter
DAP12VBD1	Housekeeping board 1 +12V converter
DAM12VBD1	Housekeeping board 1 -12V converter
DAP5VBD1	Housekeeping board 1 +5V converter
DAP15VBD2	Housekeeping board 2 +15V converter
DAM15VBD2	Housekeeping board 2 -15V converter
DAP12VBD2	Housekeeping board 2 +12V converter
DAM12VBD2	Housekeeping board 2 -12V converter
DAP5VBD2	Housekeeping board 2 +5V converter
DABD1V	Housekeeping board 1 ref. voltage
DARREF1BD1	Housekeeping board 1 ref. resistance #1
DARREF2BD1	Housekeeping board 1 ref. resistance #2
DABD2V	Housekeeping board 2 ref. voltage
DARREF1BD2	Housekeeping board 2 ref. resistance #1
DARREF2BD2	Housekeeping board 2 ref. resistance #2
DASPARE1	Spare

B.2.9 PDU Voltages

Mnemonic	Description
DPFP7.2V	FPA HEMT regulator +7.2V converter
DPFM7.2V	FPA HEMT regulator -7.2V converter
DPRP7.2V	RXB HEMT regulator +7.2V converter
DPRM7.2V	RXB HEMT regulator -7.2V converter
DPFLEDP10V	LED +10V converter voltage
DPPHSWCONVP9V	Phase switch driver +9V converter
DPPHSWCONVM9V	Phase switch driver -9V converter
DPFLDAP6.2V	Line driver A, DAs 1-5 +6.2V converter
DPFLDAM6.2V	Line driver A, DAs 1-5 -6.2V converter
DPFLDBP6.2V	Line driver B, DAs 6-10 +6.2V converter
DPFLDBM6.2V	Line driver B, DAs 6-10 -6.2V converter
DPHKP15V	Housekeeping +15 V converter
DPHKP5V	Housekeeping +5 V converter
DPHKM15V	Housekeeping -15 V converter

Appendix C

Acronym List

°C	[degree centigrade]
A	[amp]
A-hr	[amp hour]
A/D	Analog to Digital
A/C	Air Conditioning
AC	Alternating Current
ACE	Attitude Control Electronics
ACS	Attitude Control System
AEU	Analog Electronics Unit
ANSI	American National Standards Institute
AO	Announcement of Opportunity
AOS	Acquisition of Signal
APID	Application Process Identification
ASIC	Application Specific Integrated Circuit
ASIST	Advanced System for Integration and Spacecraft Testing
ASQC	American Society for Quality Control
AST	Autonomous Star Tracker
ATC	Active Thermal Control
ATS	Applications Technology Satellite
	Absolute Time Sequence
AWG	American Wire Gauge
AWS	Associate Work Station
BB	Breadboard
BER	Bit Error Rate
BIB	Bus Interface Box
BOA	Beginning of Activity
BOL	Beginning of Life
BOT	Beginning of Track
bps	[bits per sec]
BPT	Business Product Team
BSOC	Battery State of Charge
BTE	Bench Test Equipment

BWG	Beam Wave Guide
BW	Bandwidth
C&DH	Command & Data Handling
CADU	Channel Access Data Unit
CCAS	Cape Canaveral Air Station
CCB	Configuration Control Board
CCD	Charge Coupled Device
CCR	Configuration Change Request
CCSDS	Consultative Committee for Space Data & Systems
CCT	Close Circuit Television
CDR	Critical Design Review
CG	Center of Gravity
CGS	Combined Ground System
CIRS	Composite Infrared Spectrometer
CLA	Coupled Loads Analysis
CLK	Clock
CMB	Cosmic Microwave Background
CMD	Command
CM	Configuration Management
CMS	Command Management System
CNT	Count
COBE	Cosmic Background Explorer
COI	Composite Optics, Inc.
COP-1	Command Operations Procedure #1
COTS	Commercial Off-the-Shelf
CPT	Comprehensive Performance Test
CPV	Common Pressure Vessel
CQ	Command Quaternion Target
CQT	Command Quaternion Table
CRC	Cyclic Redundancy Check
CSLP	Cooperative Satellite Learning Project
CSS	Coarse Sun Sensor
CT1	Cold Test #1 (of CVC Test)
CT2	Cold Test #2 (of CVC Test)
CTE	Coefficient of Thermal Expansion
CTT	Compatibility Test Trailer
CUC	CCSDC Unsegmented Time Code
CVC	Cold-Vibe-Cold
CVCDU	Coded Virtual Channel Data Unit
CVCM	Collected Volatile Condensable Material
CVT	Current Value Table
CY	Calendar Year
D/A	Digital to Analog
D/NAR	Design/Non-Advocate Review
DA	Differencing Assembly
DAC	Digital/Analog Converter
dB	[decibel]
dBi	[decibel relative to an isotropic distribution]
DBS	DBS Microwave, Inc.

dBw	[decibel relative to one watt]
DC	Direct Current
DDD	DSN Data Delivery
DDTE	Design, Development, Test, and Evaluation
DEU	Digital Electronics Unit
DHDS	Digital History Data Storage
DMR	Differential Microwave Radiometer Detailed Mission Requirements
DoD	Depth of Discharge
DSCC	Deep Space Communications Complex
DSOC	DSN Space Operations Center
DSN	Deep Space Network
DSPT	Data Systems Product Team
DSSE	Digital Sun Sensor Electronics
DSS	Digital Sun Sensor
DFT-21	Development and Test Facility - 21
DTO	Detailed Test Objective
EDAC	Error Detection and Correction
EEE	Electrical, Electronics and Electromechanical
EEPROM	Electrically Erasable Programmable Read Only Memory
EIRP	Equivalent Isotropically Radiated Power
EMC	Electromagnetic Compatibility
EMI	Electromagnetic Interference
EOL	End Of Life
EOM	End of Mission
EO	Engineering Order
EO-1	Earth Observer-1
EOP	End of Pass
EOT	End of Track
EPT	Electrical Product Team
EPV	Extended Precision Vector
ESD	Electrostatic Discharge
ESN	Essential Services Node
ER	Established Reliability
ETF	Environmental Test Facility
ETR	Eastern Test Range
ET	Established Time
ETU	Engineering Test Unit
EU	Engineering Unit
EVD	Engine Valve Driver
FAM	Flight Assurance Manager
FAR	Federal Acquisition Regulations
FAST	Fast Auroral Snapshot Explorer
FDC	Fault Detection and Correction
FDf	Flight Dynamics Facility
FEDS	Front-End Data System
FEM	Finite Element Model
FET	Field Effect Transistor
FIRS	Far Infrared Survey

FlatSat	WMAP Spacecraft Simulator Facility (GSFC)
FMEA	Failure Modes and Effects Analysis
FORTTRAN	FORmula TRANslation
FOT	Flight Operations Team
FPA	Focal Plane Assembly
FSDF	Flight Software Development Facility
FSW	Flight Software
FSWM	Flight Software Maintenance Team
FRR	Flight Readiness Review
FTP	File Transfer Protocol
FWHM	Full Width at Half Maximum
FY	Fiscal Year
G&A	General & Administrative
G/O	Gain Offset
GaAs	Gallium Arsenide
GAC	Gamma-Alumina Cylinder
Gbit	[gigabit]
GCI	Geocentric Inertial
GEO	Geosynchronous Earth Orbit
GHe	Gaseous Helium
GHz	[gigahertz]
GMT	Greenwich Mean Time
GN	Ground Network
GN2	Gaseous Nitrogen
GND	Ground
GOS	Geomagnetic Observing System
GSE	Ground Support Equipment
GSFC	Goddard Space Flight Center
GTDS	Goddard Trajectory Determination System
GUI	Generic User Interface
H&S	Health and Safety
H/W	Hardware
HDF	Hierarchical Data Format
HEALPix	Hierarchical Equal Area isoLatitude Pixelisation
HEMT	High Electron Mobility Transistor
HFSS	High Frequency Structure Simulator
Hg	Mercury
HiFi	High Fidelity Simulation
HK	Housekeeping
HPBW	Half Power Beam Width
hr	[hour]
HVAC	Heating, Ventilating and Air Conditioning
Hz	[hertz]
I&T	Integration & Test
I&V	Integration & Verification
I/F	Interface
I/O	Input/Output
IC	Integrated Circuit
ICD	Interface Control Document

IDEAS	Information Development and Applications, Inc.
ID	Identification
IDL	Interactive Data Language
IDR	Instrument Design Review
IGSE	Instrument Ground Support Equipment
IHK	Instrument Housekeeping
IITA	Information Infrastructure Technology and Applications
IMAGE	Imager for Magnetopause-to-Aurora Global Exploration
IMAPS	Interstellar Medium Absorption Profile Spectrograph
in ³	[cubic inch]
in	[inch]
InP	Indium Phosphide
IOC	Initial Operational Capability Initial Orbiting Configuration In-Orbit Checkout
IPM	Instrument Project Manager
IP	Internet Protocol
IR	InfraRed
IRU	IVA Replacement Unit Inertial Reference Unit
ISE	Instrument Systems Engineer
Isp	Specific Impulse [s]
ITO	Indium-Tin-Oxide
IUE	International Ultraviolet Explorer
JPL	Jet Propulsion Laboratory
JURAP	Joint User Resource Allocation Panel (DSN)
kbps	[kilobits per second]
kg	[kilogram]
kHz	[kilohertz]
K	[kelvin]
KF	Kalman Filter
km	[kilometer]
KSC	Kennedy Space Center
kw	[kilowatt]
L&IOC	Launch & In-Orbit Checkout
L1	First Sun-Earth Libration (Lagrange) Point
L2	Second Sun-Earth Libration (Lagrange) Point
LAN	Local Area Network
lbf	[pounds, force]
lbm	[pounds, mass]
LED	Light-Emitting Diode
LEE	Lightweight Electronics Enclosure
LEISA	Linear Etalon Imaging Spectrometer Array
LEO	Low Earth Orbit
LET	Linear Energy Transfer
LF	Launch Facility
LHe	Liquid Helium
LLV	Lockheed Launch Vehicle
LMAC	Little MIDEX Attitude Control Electronics

LOS	Loss of Signal Line of Sight
LN2	Liquid Nitrogen
LOX	Liquid Oxygen
LRR	Launch Readiness Review
LVPC	Low Voltage Power Controller
LV	Launch Vehicle
m	[meter]
M_PDU	Multiplexing Protocol Data Unit
MAC	Maximum Allowable Concentration MIDEX Attitude Control (Electronics)
MATLAB®	Matrix Laboratory
MAP	Microwave Anisotropy Probe
MAR	MIDEX Assurance Requirements
MAX	Microwave Anisotropy Experiment
Mbps	[megabits per second]
MCC	Mid-Course Correction
MCM	Multi Chip Module
MDM	Multiplexer/Demultiplexer
Mdot	Mass Flow Rate
MECO	Main Engine Cut Off
MEOP	Maximum Expected Operating Pressure
MET	Mission Elapsed Time
MGA	Medium Gain Antenna
MHz	[megahertz]
MICM	Multi-variable Instrument Cost Model
MIDEX	Medium-Class Explorer
MIL-71	DSN Merritt Island Testing Facility
MILA	Merritt Island Station (GN)
MITOC	MAP Integration and Test Operations Center
MLI	Multi Layer Insulation
MMFD	Multi-Mission Flight Dynamics
MPPF	Multi-Payload Processing Facility
MO&DA	Mission Operations & Data Analysis
MOC	Mission Operations Center
MPI	Message Passing Interface
MPS	Multi-Program Support
MPT	Microwave Product Team
MRR	Mission Requirements Review Mission Readiness Review
MRT	Mission Readiness Test
MS	Microwave System
ms	[millisecond]
MSAM	Medium Scale Anisotropy Measurement
MSX	Mid-Course Space Experiment
MV	Mongoose 5; [megavolt]
N	[newton]
N2H4	Hydrazine
NASA	National Aeronautics and Space Administration

NASCAP	NASA Surface Charging Analysis Program
NAVGSE	Navigational Ground Support Equipment
Nch	Number of Channels
ND	Network Director
NHB	NASA Handbook
NISN	NASA Integrated Services Network
Nms	Newton Meter Seconds
NOCC	Network Operations Control Center (DSN)
NRAO	National Radio Astronomy Observatory
NRZ-L	Non-Return to Zero-Level
NSF	National Science Foundation
NSPAR	Non-Standard Parts Approval Request
NSSDC	National Space Science Data Center
OC	Operations Center
OD	Orbit Determination
OMEGA	Office of the MAP Experiment General Archive
OMNI	Omni-directional Antenna
OMT	Orthomode Transducer
OPM	Orbital Parameter Message
OS	Operating System
PAF	Payload Adapter Fitting
PB	Playback
Pc	Thrust Chamber Pressure
PC	Printed Circuit; Personal Computer
PCA	Proportional Counter Array
PCB	Printer Circuit Board
PCI	Programmed Composites, Inc.
PD	Proportional and Derivative
PDR	Preliminary Design Review
PDT	Product Development Team
PDU	Power Distribution Unit
PEB	Parts Evaluation Board
PER	Pre-Environmental Review
PERT	Program Evaluation and Review Technique
PFR	Problem/Failure Report
PFU	Proto-flight Unit
PHSF	Payload Hazardous Servicing Facility
PI	Principal Investigator
PIND	Particle Impact Noise Detection
pixel	picture-element
PM	Project Manager, Phase Modulation
PN	Pseudo-Random Noise Coding
POC	Point of Contact
POP	Program Operating Plan
PROM	Programmable Read Only Memory
PR	Problem Report
PRT	Platinum Resistance Thermometer
PSE	Power Supply Electronics
psia	[pounds per square inch, absolute]

psig	[pounds per square inch, gauge]
PSK	Phase Shift Keying
PSLA	Project Service Level Agreement
PSR	Pre-Ship Review
PS	Phase Switch
PTF	Pressure Transducer and Filter
	Portable Telemetry Formatter
PU	Princeton University
PWM	Pulse Width Modulator
PWS	Primary Work Station
QA	Quality Assurance
QTM	Qualification Test Model
R/D	Reed-Solomon
RAAN	Right Ascension of the Ascending Node
RAM	Random Access Memory
RAO	Resources Analysis Office
RCS	Reaction Control System
RCVR	Receiver
RDL	Record Definition Language
RE	Earth Radius
REU	Reflector Evaluation Unit
RF	Radio Frequency
RFI	Radio Frequency Interference
RFP	Request for Proposal
RFSOC	Radio Frequency Simulations Operations Center
RID	Review Item Discrepancy
RISC	Reduced Instruction Set Computing
RM	Resources Manager
RMS	Root Mean Square
ROM	Read Only Memory
REV	Revolutions
ROSAT	Roentgen Satellite
rpm	[revolutions per minute]
RR	Requirements Review
RSI	Research Systems, Inc.
RSN	Remote Services Node
RS	Solar Radii
	Radiated Susceptibility
RSS	Root-Sum-Square
RTS	Relative Time Sequence
	Range Tracking Station
RT	Real Time
RWE	Reaction Wheel Electronics
RW	Reaction Wheel
RWA	Reaction Wheel Assembly
RXB	Receiver Box
s	[second]
S&MA	Safety & Mission Assurance
S/C	Spacecraft

SA	Solar Array
SAA	South Atlantic Anomaly
SADEB	Solar Array Deployment Electronics Box
SAEF-2	Spacecraft Assembly and Encapsulation Facility #2
SAM	Solar Array Module
SAMPEX	Solar Anomalous and Magnetospheric Particle Explorer
SAS	Solar Array Simulator
SCAPE	Self Contained Atmospheric Personnel Ensemble
SCC	Standard Cubic Centimeter
SCOPR	Systems Concept & Operating Plan Review
SCR	Spacecraft Concepts Review System Concept Review
SCT	Spacecraft Controller Team
SDSS	Sloan Digital Sky Survey
SDT	Spacecraft Development Team
SECO	Second-Stage Engine Cutoff
SEE	Single Event Effect
SEIT	Systems Engineering & Integration Team
SERS	Spacecraft Emergency Response System
SERTS	Solar Extreme-UV Rocket Telescope Spectrograph
SEU	Single Event Upset
SFDU	Standard Formatted Data Unit
SIGI	Silicon Graphics, Inc.
SGSE	Spacecraft GSE
SH	Safe Hold
SHOOT	Superfluid Helium On-Orbit Transfer
SICM	Scientific Instrument Cost Model
SiO	Silicon Oxide
SK	Station Keeping
SLC	Space Launch Complex
SMEX	Small Explorer Program
SMM	Solar Maximum Mission
SMOC	Science and Mission Operations Center
SN	Space Network
SOH	State of Health
SOHO	Solar and Heliospheric Observatory
SPS	Small Purchase System
SPSS	Science Planning and Scheduling System
SRM	Solid Rocket Motor
SSR	Solid State Recorder
SS	Subsystem; Steady States; Stainless Steel
SSTI	Small Spacecraft Technology Initiative
STK	Satellite Tool Kit
STM	Structural/Thermal Model
STOL	Spacecraft Test and Operations Language
STOP	Structural/Thermal Optical
STPT	Structural/Thermal Product Team
STSci	Space Telescope Science Institute
ST	Star Tracker

SWAS	Submillimeter Wave Astronomy Satellite
SWG	Science Working Group
TARA	Two Axis Rate Assembly
TBD	To Be Determined
TBR	To Be Resolved; To Be Required; To Be Refined
TBS	To Be Specified; To Be Supplied
TCP/IP	Transmission Control Protocol/Internet Protocol
TCS	Thermal Control System
TDI	Time Delay Integration
TDRS	Tracking and Data Relay Satellite
TEC	Thermo-Electric Cooler
Ti	Titanium
TID	Total Ionizing Dose
TIF	Timing & Interference
TLM	Telemetry
TML	Total Mass Loss
TOD	Time of Day; True of Date
TOMS-EP	Total Ozone Mapping Spectrometer-Earth Probe
TOTS	Transportable Orbital Tracking Station
TOT	Table of Tables
Transistor	TRANSfer-reSISTOR
TRMM	Tropical Rainfall Measuring Mission
TRS	Thermal Reflector System
TSM	Telemetry and Statistics Monitor
Tsys	System Noise Temperature
TTI	Transfer Trajectory Insertion
TURFTS	TDRS User RF Test Set
UBC	University of British Columbia
UCLA	University of California Los Angeles
UPR	User Problem Report
UTMC	United Technologies Microprocessor Chip
V	Velocity; [volt]
V/F	Voltage-to-Frequency
V/T	Voltage/Temperature
	Voltage/Taper
VC	Virtual Channel
VCDU	Virtual Channel Data Unit
VDA	Vapor-Deposited Aluminum
VDC	[volt, direct current]
VDS	Voice Distribution System
VLSI	Very Large Scale Integration
VPF	Vertical Processing Facility
VRAIL	Voltage Regulator and In-Rush Limiter
VR	Virtual Recorder
W	[watt]
WBS	Work Breakdown Structure
WIND	Solar Wind Mission
WMAP	Wilkinson Microwave Anisotropy Probe
WSC	White Sands Complex

WS	Workstation
WTR	Western Test Range
XCAL	External Calibrator
XDS	XRS Detector System
XPDR	Transponder
XRSN	Transponder RSN
XRS	X-ray Spectrometer
XTE	X-ray Timing Explorer
YRS	[year]
ΔH	Change in Angular Momentum [Nms]
ΔV	Delta-V, Change in Velocity [m/s]
Ω	[ohm]